TOPICAL REPORT

Geophysical Study of the Monroe-Red Hill

Geothermal System

by

Charles W. Mase, David S. Chapman and S. H. Ward

Work performed under Contract No.

EY-76-S-07-1601

Department of Geology and Geophysics

University of Utah
Salt Lake City, Utah (USA)

October 1978

Prepared for
DEPARTMENT OF ENERGY
Division of Geothermal Energy

Geophysical Study of the Monroe-Red Hill

Geothermal System

by

Charles W. Mase, David S. Chapman and S. H. Ward

October 1978

Geophysical Study of the Monroe-Red Hill

Geothermal System

ABSTRACT

A detailed geophysical study consisting of heat flow,
dipole-dipole resistivity, ground magnetics and gravity was conducted
in the vicinity of Monroe, Utah to assess the resource potential of an
identified hydrothermal system. The detailed study covered a 40 km^2
area along the Sevier fault near the Monroe-Red Hill hot springs.
Fourteen 100m dipole-dipole resistivity profiles across the system
were used to construct a first separation apparent resistivity contour
map. The map effectively outlines the trace of the Sevier fault and
reveals an elongate zone of low resistivity (<10 Ω-m) associated with
the hydrothermal system. Similar features are evident on the total
magnetic intensity anomaly map. Gravity modeling across the system
indicates that the Sevier fault is comprised of three or more nearly
vertical en echelon faults. On the basis of geological mapping and
surface geophysical surveys a series of eleven shallow boreholes
(40-90m) was drilled on two profiles across the system. Surface
geothermal gradients vary from 240°C km^{-1} to over 1000°C km^{-1} along
the profiles. Heat flow values vary smoothly from 550 mW m^{-2} to over
3000 mW m^{-2}, a significant enhancement over background Basin and Range
heat flow of 80 mW m^{-2}. Heat budget calculations based on conductive
heat loss and enthalpy of the discharge waters indicate a net power
loss of 7.8 MW.

Models of the system picture the deep circulation and heating of

groundwater and subsequent discharge to the surface through the Sevier fault zone. The lack of Pleistocene and Quaternary volcanism in the area suggests that the system is a stable stationary phase supported by high regional heat flow and forced convection.

TABLE OF CONTENTS

LIST OF ILLUSTRATIONS

Figures

LIST OF ILLUSTRATIONS (cont.)

TABLES

INTRODUCTION

The Monroe-Red Hill hydrothermal system occupies the eastern
flank of the central Sevier River Valley, immediately east of the town
of Monroe, Utah. The springs issue from the Sevier fault which is a
major west-dipping normal fault marking the western termination of the
Sevier Plateau against the alluvial fill of the Sevier River Valley.

The region surrounding the Monroe-Red Hill hydrothermal system
has been the object of concerted geological, geochemical and
geophysical studies by the University of Utah on behalf of the
Department of Energy, Division of Geothermal Energy. The first
detailed studies of these hot springs (Parry et al., 1976; Miller,
1976) were concerned with the geochemistry and alteration mineralogy
of the system and provide valuable constraints on the origin and
history of the thermal waters. During the summer of 1977, and
extending into 1978, a detailed geophysical study consisting of heat
flow, dipole-dipole resistivity, ground magnetics and precision
gravity (Halliday, 1978) was conducted to assess the resource
potential of the hydrothermal system. The detailed study covered a 40
km^2 area along the Sevier Fault near the Monroe and Red Hill hot
springs.

The present work was undertaken to delineate more clearly the
extent of the subsurface thermal features, to determine the thermal
structure of the system, and to ascertain the nature and origins of
the thermal fluids and heat sources. This information provides the
basis for determining whether the system represents an adequate

resource for use in space heating for the town of Monroe. Moreover, the study will aid in explaining the nature of the many geothermal systems lying along major range front faults in the Basin and Range Province.

BACKGROUND DATA

Geology

The central Sevier River valley is situated within the Basin and
Range-Colorado Plateau transition province in central Utah. It is an
alluvial filled intermontaine valley bounded on the east by the Sevier
Plateau and on the west by the Pavant Range. The Sevier Plateau with
its gently sloping summit area more nearly resembles the plateau lands
to the east, while the Pavant Range with its many structural features
is more characteristic of the Basin and Range. A general geologic map
of the central Sevier Valley region is illustrated in figure 1. The
geologic information in the figure is generalized from Callaghan and
Parker (1961), Stokes and Hintze (1963), Young and Carpenter (1965),
and Hahl and Mundorff (1968).

Tertiary volcanics are the dominant rocks of the area. The
Monroe and Red Hill hot springs are located near the northern edge of
the Marysvale volcanic field, where extensive and prolonged volcanism
occurred from middle to late Tertiary. The volcanics range in
composition from basalt to rhyolite and in age from Oligocene to
Pliocene. The volcanic rocks lie upon sedimentary rocks that vary in
age from Jurassic to Oligocene, depending upon location.

The Bullion Canyon volcanics comprise the dominant rock type in
the Monroe-Red Hill area and are Miocene in age. They are comprised

RICHFIELD

Sevier Valley

Pavant Range

MONROE

Tushar Mountains

Antelope Range

Sevier Plateau

MARYSVALE

N

UTAH

Area Location Map
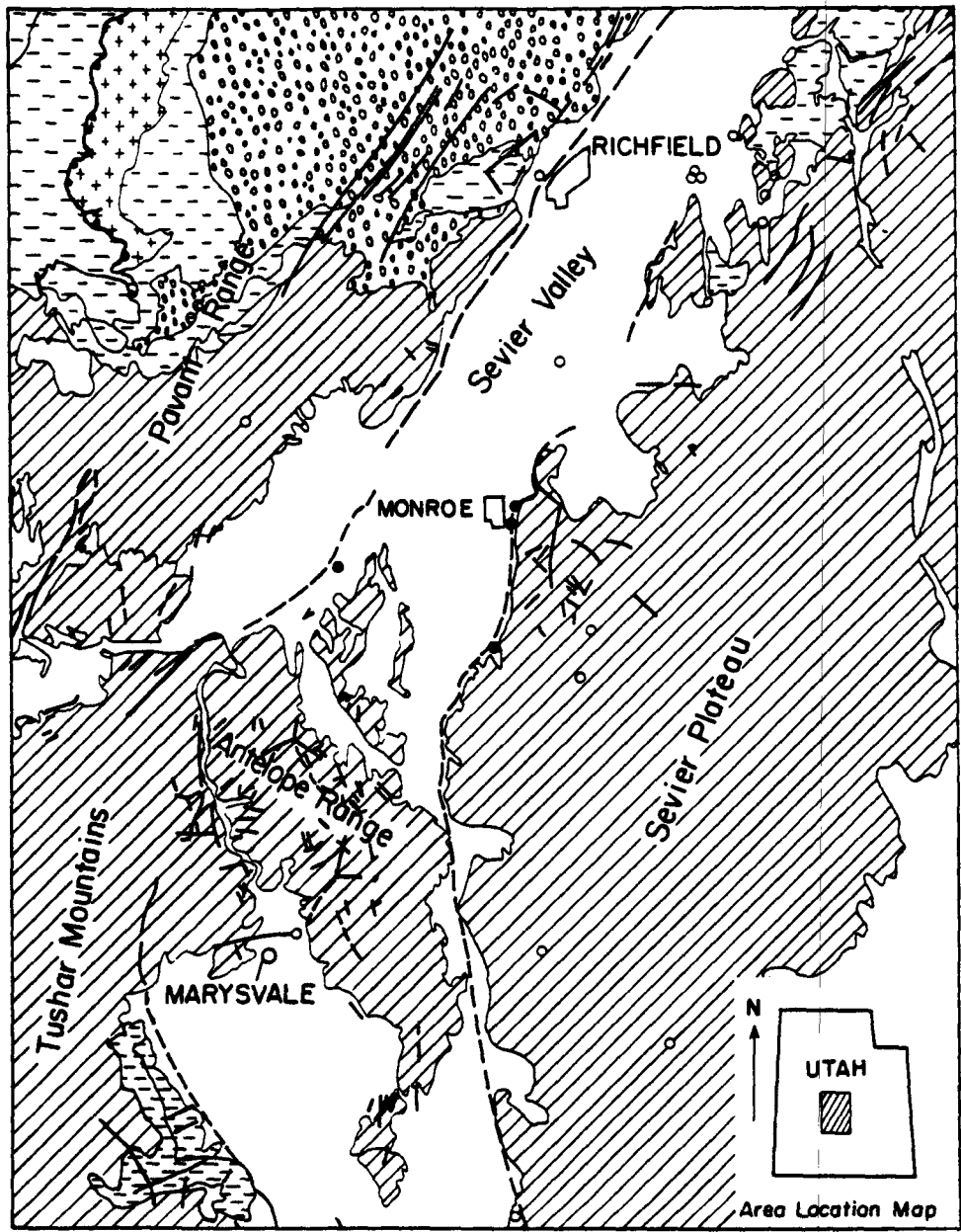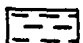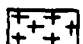
TERTIARY BULLION CANYON VOLCANICS   ● HOT SPRING

UNDIFFERENTIATED MESOZOIC SEDIMENTARY ROCKS.   ○ COLD SPRING

UNDIFFERENTIATED MESOZOIC SEDIMENTARY ROCKS.   ╱ MAPPED FAULT (DASHED WHERE INFERRED)

QUATERNARY ALLUVIUM

UNDIFFERENTIATED TERTIARY SEDIMENTARY ROCKS

Figure 1: Generalized geology of the region surrounding Monroe, Utah.

of pyroclastics in the lower part, overlain by thick porhyritic latite flows and breccias with an upper member consisting of basaltic andesite flows. The thickness of the Bullion Canyon volcanics is approximately 400 meters northeast of Richfield thickening to 1500 meters near Monroe Peak (Callaghan and Parker, 1961).

Intrusive igneous bodies of Miocene age are associated with the Bullion Canyon volcanics. The intrusions primarily consist of stocks ranging from monzonitic to granitic composition. The nearest stock to the Monroe-Red Hill system is located at Monrovian Park, three miles to the southeast. The stock is about one mile in diameter and is typical of other Miocene intrusives that have invaded the volcanics.

Underlying the Bullion Canyon volcanics are sedimentary rocks varying in age from Jurassic to Oligocene, depending on location. Their detailed stratigraphy and structure underneath the volcanic pile at Monroe is not known. The Mesozoic and older sedimentary rocks have been folded and thrust faulted (Hardy, 1952). All of the rocks, including the volcanics, were faulted and fractured during Basin and Range normal faulting, which began during Miocene times and has continued sporadically to the present.

The Jurassic Arapien shale locally underlies the Bullion Canyon volcanics east of Richfield and southwest of Marysvale. It is composed of stratified salts, lenticular gypsum beds and thin bedded limestones and shales. This formation obtains a maximum thickness of 760 meters in outcrop between Gunnison and Richfield before it disappears beneath the volcanic cover. Southwest of Marysvale the Arapien shale is only a veneer indicating that the unit thins rapidly

southward beneath the volcanic cover at Monroe. Southeast of Kanosh
in the Pavant Range, the volcanics are underlain by a veneer of
Tertiary and Cretaceous sediments, which overlie the Jurassic Navajo
sandstone. The Navajo sandstone underlies the Arapien shale
stratigraphically and has an estimated thickness of 400m (Stokes and
Hintze, 1973). The geologic evidence suggests that the region of the
Sevier plateau may have been an antiform during the Cretaceous and
early Tertiary, upon which sediments of this age were either not
deposited or deposited and subsequently eroded away before the
extrusion of the Bullion Canyon volcanics onto Jurassic age sediments.

Figure 2 represents an idealized east-west geologic cross section
near Monroe. The Sevier valley floor is formed of narrow, down-
dropped fault blocks covered by Pliocene and Pleistocene sediments,
which vary in thickness from a veneer to as much as 500 meters (Young
and Carpenter, 1965). The fill is comprised of fanglomerates, terrace
and streambed gravels, clays and landslide debris.

High angle normal faulting is the dominant structural feature of
the Colorado Plateau - Basin and Range transition province and is
responsible for many of the topographic features as well. The Sevier
fault zone from which the hot springs issue is mostly buried by
alluvium and has been inferred in most localities to be near the
western termination of the Sevier Plateau against the alluvial fill of
the Sevier River valley. Other major range front faults in the area
include the Elsinore and Dry Wash faults, which mark the western
termination of the synclinal valley in which Monroe sits. The Joseph

W   SEVIER FAULT   E

SEVIER PLATEAU

SEVIER RIVER VALLEY

DEPTH (km)

TQal

Tjl

Tb

Ja

Tb

Ja

Jn

MP

DISTANCE (km)

VERTICAL EXAGGERATION 2:1

TQal   Alluvium

Tjl   Joe Luff Tuff

Tb   Bullion Canyon Volcanics

Ja   Arapien Shale

Jn   Nugget Sandstone

MP   Undivided Lower Mesozoics Palezoics
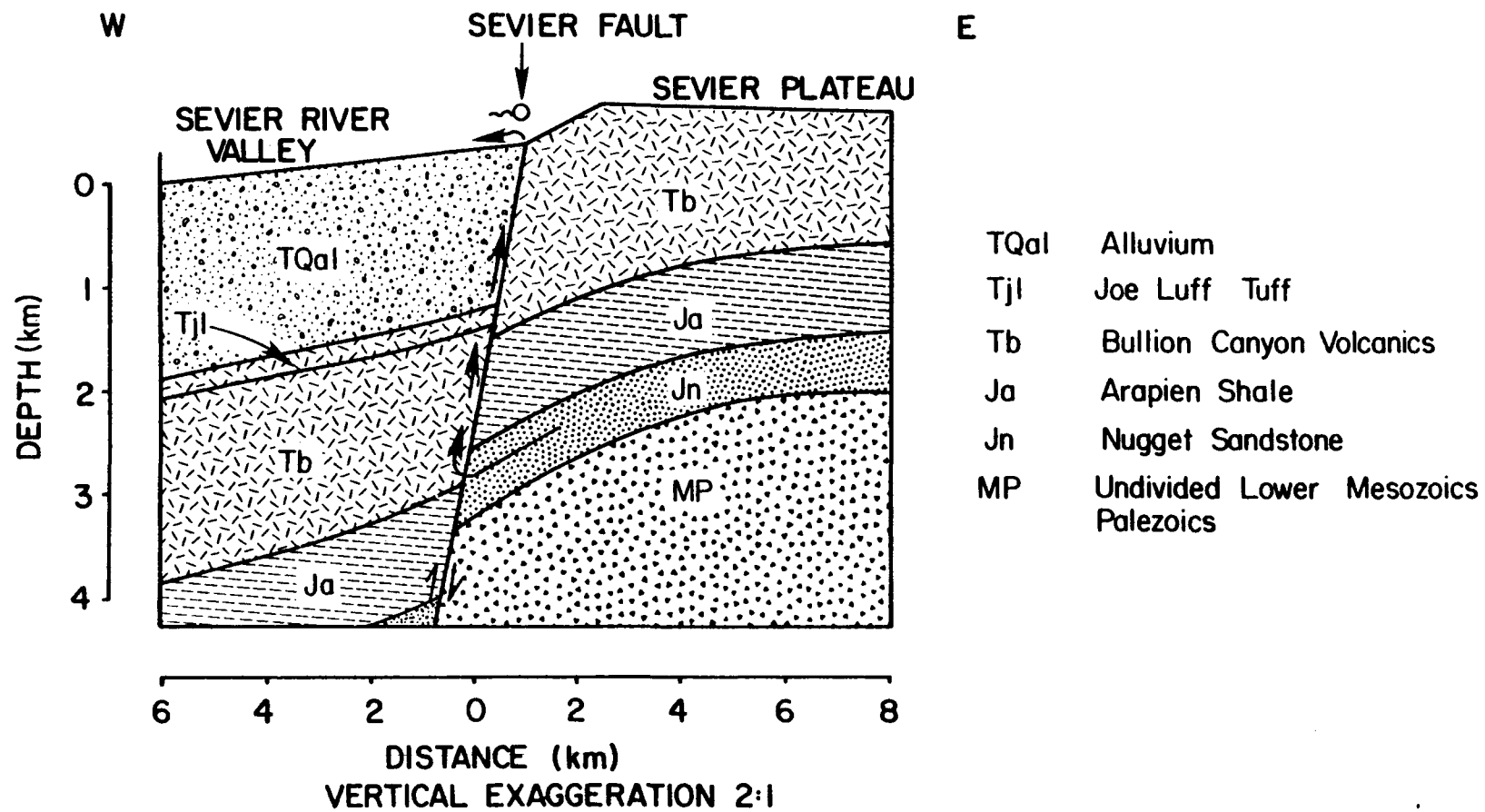
Figure 2: Generalized geologic cross section of the Sevier Fault near Monroe, Utah.

hot springs issue from the Dry Wash fault.

Geothermal manifestations along the Sevier fault are indicated by the bright red travertine deposits at Red Hill, the kidney-shaped tufa mound at Monroe Hot Springs, and the visible alteration at Johnson warm springs. The springs occur at apparent changes in the trend of the surface trace of the Sevier fault.

Geochemistry

Na-K-Ca and silica geothermometers indicate temperatures of last wall rock equilibration of 187°C and 104°C (Parry et al., 1976), respectively, for the thermal fluids. The Na-K-Ca geothermometer may be considered unreliable because the hot spring water may have acquired its salinity from evaporites within the Arapien shale. From geochemistry, Parry et al. (1976) determined that the spring waters are most likely a mixture of a hot saline component and a cool component that is chemically similar to surface water in the area. A mixing model, based on the measured silica content of the warm water and the warm water enthalpy, indicate a mixture of 62% hot water at 118°C and 38% cold water at 10°C. In normal Basin and Range terrain with a heat flow of 80 mW m^{-2}, this temperature is reached between 2.0 and 4.0 km , depending on rock type and thermal conductivity. The aquifer that constitutes the hot fluid reservoir may be the Jurassic Navajo sandstone which is generally permeable and lies beneath the volcanic cover. The location of mixing between the hot and cold waters is speculative, but may take place at the intersection of the Sevier fault with the basaltic andesite flows of the Bullion

Canyon volcanics, the contact between the Jurassic Arapien shale and Bullion Canyon volcanics, or the limestone beds contained within the Arapien shale. Kilty et al. (1978) speculate that this mixing zone may be as shallow as 500 meters, but the actual depth is unknown.

Geologic Model

The lack of Pleistocene and Quaternary volcanism suggests that a magmatic intrusion is an unlikely explanation for the heat source. The geology and geochemistry indicates that deep circulation, storage and heating within a reservoir due to a normal Basin and Range heat flow with subsequent discharge to the surface through the Sevier fault zone is more likely. Figure 2 represents an idealized geologic cross-section through the Monroe-Red Hill system depicting the Navajo Sandstone as the hot reservoir. The recharge of the Navajo sandstone probably occurs in the highlands of the Sevier Plateau, through available fractures and faults in the overlying volcanic and sedimentary cover. A vertical piezometric gradient of 2%, equivalent to a 50m decrease in a 2.5km rise from the reservoir to the surface, is required to account for the springs discharge (Kilty et al., 1978).

GEOPHYSICAL STUDIES

Ground Magnetics

The magnetic pattern for the Monroe Hot Spring region was determined by conducting 18 profiles across the system. The total magnetic intensity was measured using a Geometrics proton precession magnetometer.

The total magnetic intensity anomaly map, figure 3, discloses a strong magnetic gradient that parallels the Sevier fault zone. Magnetic highs are associated with the alluvium and lows with the Bullion Canyon volcanics indicating that the alluvium is relatively magnetic compared to the volcanics. Magnetic susceptibilities were measured for surface outcrop samples, and cuttings and core samples obtained from thermal gradient heat flow drill holes. The Bullion Canyon volcanics within the study area consist almost entirely of latite breccias and flows with an observed average magnetic susceptibility of .0002 cgs. The alluvium has an observed magnetic susceptibility of .0015 cgs. The high susceptibility of the alluvium may be explained by the large amount of erosional detritus derived from the basaltic andesite member of the Bullion Canyon volcanics, which has an average susceptibility of .0034 cgs. Alluvium adjacent to the hot springs has a magnetic susceptibility of .0003 cgs. This low susceptibility is most probably due to the alteration of the magnetite, contained within the alluvium, to hematite by hot spring waters. Evidence of this alteration is the bright red hematite stain of the tufa mound at Red Hill.
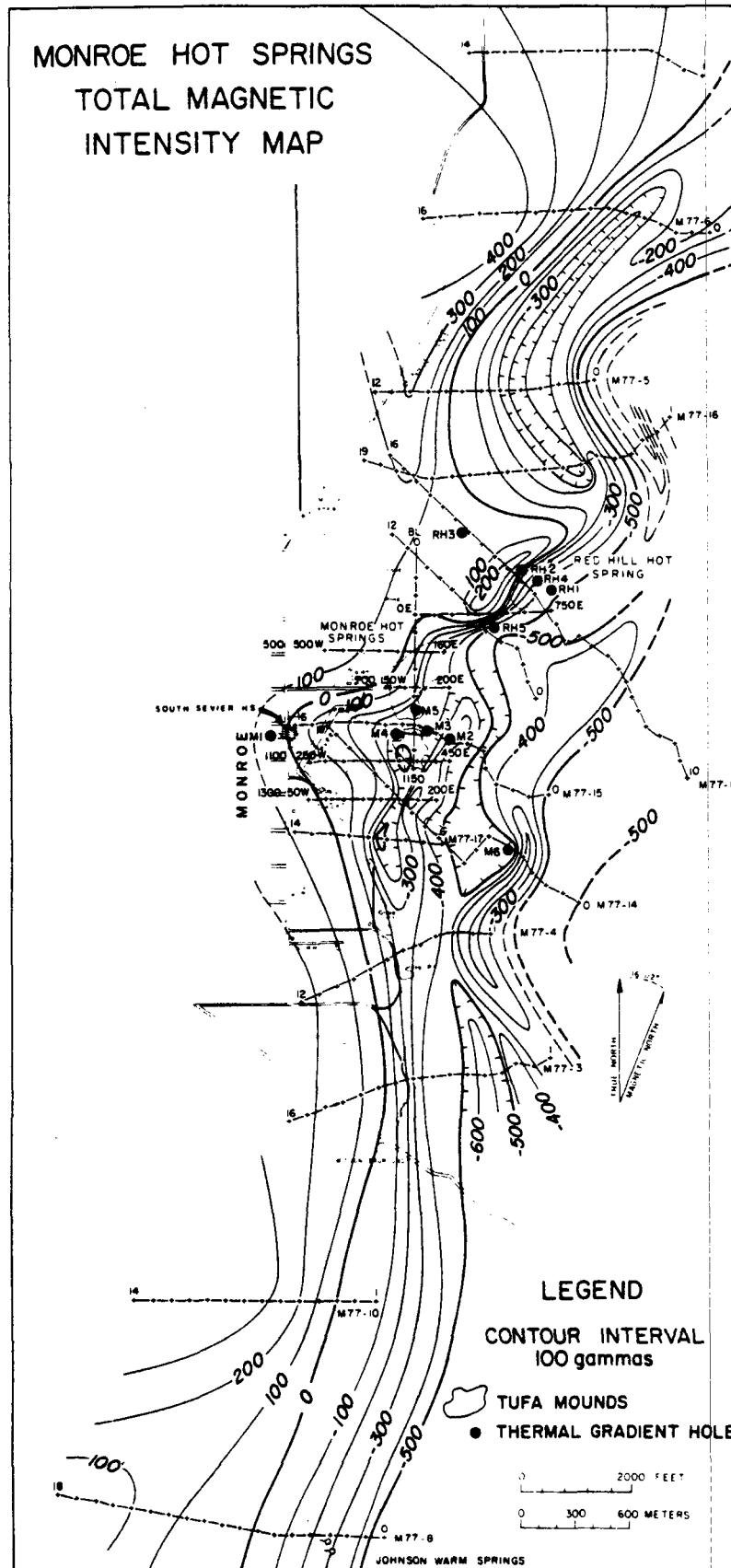
Figure 3: Total magnetic intensity anomaly map of the Monroe System.

Thus the steep magnetic gradient in Fig. 3 defines the trace of Sevier fault zone due to the contrast in magnetic properties of the alluvium on the down-thrown block versus the latite breccias and flows of the Bullion Canyon volcanics on the up-thrown block. Contained within the steep gradient at Monroe hot springs are many small lows associated with the discharge area of the hot springs. The lows are probably caused by deep cylindrical volumes where the magnetic susceptibilities are reduced nearly to zero by intense hydrothermal alteration.

Models of the subsurface magnetic response across both Monroe and Red Hill hot springs (Halliday, 1978) indicate an almost vertical magnetic contrast near the inferred surface trace of the Sevier fault and the trace as determined from geothermal gradient, heat flow drilling, and dipole-dipole resistivity. On both models this magnetic interface is located approximately 150m west of the inferred fault traces. This may be explained by the alteration of magnetite to hematite by thermal fluids creating a zone of nearly zero magnetic susceptibilities within the alluvium along the fault face. Since the volcanics on the east side of the fault have nearly zero susceptibilities the models are indicating the middle of a transition separating magnetic and non-magnetic alluvium. Magnetic methods do not serve in determining the position and attitude of the Sevier fault in the hot springs area, but only locate a transition zone of magnetic susceptibilities within the alluvium westward of the fault.

Gravity

Gravity data from Halliday (1978) were compiled to produce a gravity profile across the Monroe-Red Hill system (Fig. 4). The profile is constrained by regional data in the Sevier Valley and by precision data across the inferred fault. Unfortunately the profile is poorly constrained on the upper shoulder of the anomaly which is the region most sensitive to modeling. The estimated profile shown in figure 4 was used for comparison with calculated models.

The total Bouguer anomaly (Δg) resulting from a simple step fault or a series of step faults is given by

$$\Delta g = 2\pi G \Delta\rho h$$

where $\Delta\rho$ is the change in density across the fault zone, h is the total throw across the fault zone, and G is the universal gravitational constant. If the density contrast can be determined, then the throw on the fault is fixed and the curvature of the profile is only dependent on the geometry of the fault zone. Halliday (1978) lists densities for the Bullion Canyon volcanics which yield an average value of 2.47 gm cm^{-3}. To ensure that this value is not biased by near surface samples, the covariance between elevation and Bouguer gravity was calculated for densities ranging from 1.7 to 2.8 gm cm^{-3} (see Appendix II for details). A minimum covariance was obtained for a density of 2.5 gm cm^{-3} indicating that the average sample density of 2.47 gm cm^{-3} represents the overall density of the volcanics. Since
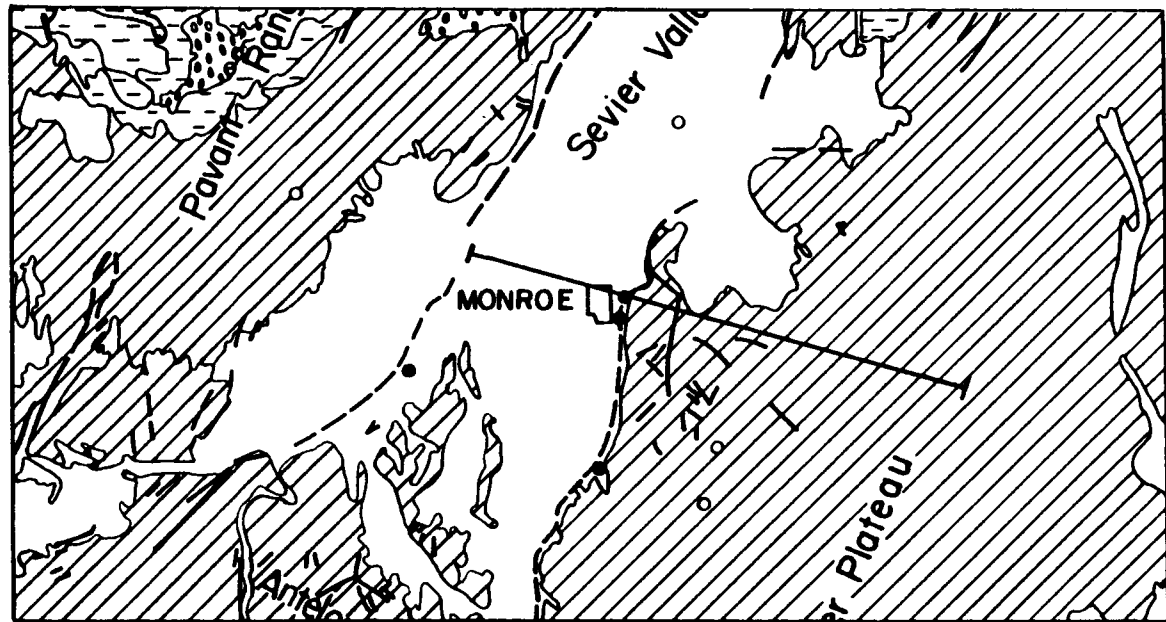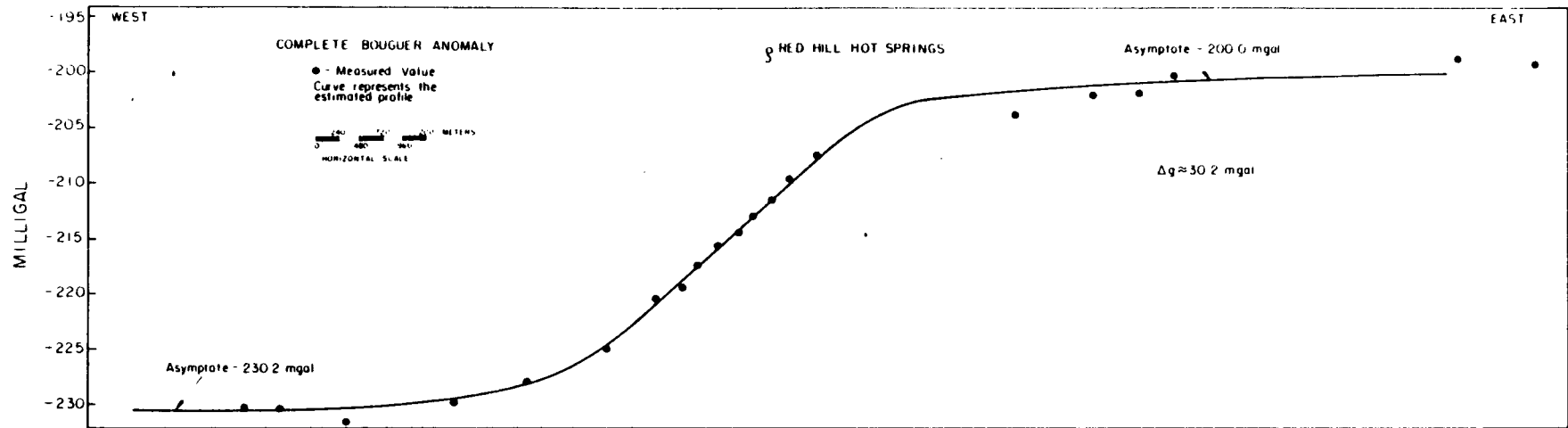
Figure 4: Complete Bouguer gravity anomaly profile across the Monroe geothermal system. Gravity data from Halliday (1978).

14

the alluvium consist entirely of erosional debris from the volcanics, the average density of the solid component must be that of the volcanics, 2.5 gm cm^{-3}. The overall density of the alluvium depends on the density of the solid component and the formation porosity. A porosity of 32% was estimated from the resistivity models through Archie's Law knowing the ionic strength of the thermal fluids saturating the alluvial gravels. A porosity of 32% also agrees well with the published values for alluvial gravels (Davis and DeWeist, 1966; Manger, 1963). This porosity yields a density contrast of 0.44 gm cm^{-3} resulting in a throw of 1760 meters across the Sevier fault zone. The calculated throw of 1760 depends on the density contrast remaining nearly constant with depth. Increases in density for depths of a few kilometers result primarily from dewatering of the sediments rather than mechanical compaction. Since the alluvium was laid down in a dry environment, compaction resulting from dewatering is likely small, and therefore the assumption of constant density contrast is reasonable.

The best fit to the data of figure 4 for a single, sloping interface ($\Delta\rho$ = 0.44 gm cm^{-3}, throw of 1760 m) had a dip of 50°. The fit was significantly better than for dips of 40° or 60°. If the density contrast is reduced to $\Delta\rho$ = 0.23 g cm^{-3} (corresponding to 20% porosity) and the throw increased, the best fitting dip increased to about 60°. The surface position of the interface in both cases was constrained to the surface trace of the Sevier fault.

The dip of this interface may not be the same as the dip of the fault since the interface may be composed of step faults. We

TWO DIMENSIONAL MODEL OF THE GRAVITY RESPONSE ACROSS THE SEVIER FAULT

COMPLETE BOUGER (mgal)

-200, -205, -210, -215, -220, -225, -230

RED HILL HOT SPRING

Estimated Profile
Calculated Values

0   1   2   3 Km
Horizontal Scale

INTERPRETATIVE GEOLOGIC CROSS-SECTION

0   1   2   3 Km.
Horizontal Scale

SURFACE

RED HILL HOT SPRING

DATUM

50°

ALTERED VOLCANICS
(2.37 gm/cm³)

Qal
(2.03 gm/cm³)

BULLION CANYON VOLCANICS
(2.47 gm/cm³)

NO VERTICAL EXAGGERATION

Figure 5:   Gravity model for profile across the Monroe geothermal system.

16

broke the interface into en echelon segments and tested the fit for various dips of the segments. The best fit was obtained with three vertical segments. Each segment had a throw of 590 m and each was separated from adjacent segments by 740 m. While the fit improved with increasing dip of the segments, the difference in fit between 70° and vertical is not significant. The fit was further improved when we included a zone of lower density material, perhaps representing hydrothermally altered and/or fractured volcanics in the upper 600 meters of volcanic rock near the fault zone. We conclude that there are probably three or more major en echelon segments to the fault which have a dip of $80^o \pm 10^o$. A satisfactory model for the gravity profile is shown in figure 5.

Dipole-Dipole Resistivity

Inferences about the lateral extent of the hydrothermal system and subsurface environment may be obtained from electrical resistivity. The resistivity of rocks in a given geothermal environment is due to two main conduction mechanisms. These mechanisms are electrolytic conduction through pore passages and fractures, and surface conduction along mineral faces and clays. Their importance has been described by Ward and Sill (1976). Electrolytic conduction obeys Archie's law

$$\rho_r = \rho_\omega \phi^{-m}$$

where the bulk rock resistivity, ρ_r, is proportional to the fractional

porosity, ϕ, and resistivity of the pore fluid, ρ_ω. The cementation factor, m, is dependent on the degree of rock consolidation and is usually near 2.0 (Brace, 1977; Keller and Frischneckt, 1966). The porosity value used in (1) is that of total rock porosity. However, only the interconnected pore spaces which contribute to current flow should be used in this term. This is generally less than the total porosity. If clays are present either as alteration products due to hydrothermal alteration or as silts in the alluvium they may lower apparent resistivities by as much as a factor of four (Ward and Sill, 1976) due to surface conduction effects. Zones of low resistivity in a geothermal environment such as Monroe-Red Hill are probably caused by a higher dissolved solid content of the thermal waters versus ground water, higher clay content due to hydrothermal alteration, increased fracture density (higher permeability within the fault zone) and the high temperature of the thermal fluids.

Geochemical analysis of the Monroe and Red Hill waters indicate that these waters are very similar electrically. Both springs have similar ionic strengths near 6.5×10^{-2} (Parry et al., 1976) which is equivalent to a .12N NaCl solution and yields a resistivity of 0.60 Ω-m for the thermal fluids at the observed discharge temperatures of 75°C (Keller and Friscneckt, 1966). Alluvial gravels with an average porosity of 35% (Davis and DeWeist, 1966; Manger, 1963) saturated with these fluids would have an apparent resistivity of 5 Ω-m. Once these thermal fluids have cooled to groundwater temperatures (10°C) the alluvium containing them would have an apparent resistivity of 15 Ω-m. Bullion Canyon volcanics with a porosity of 6% would have an apparent
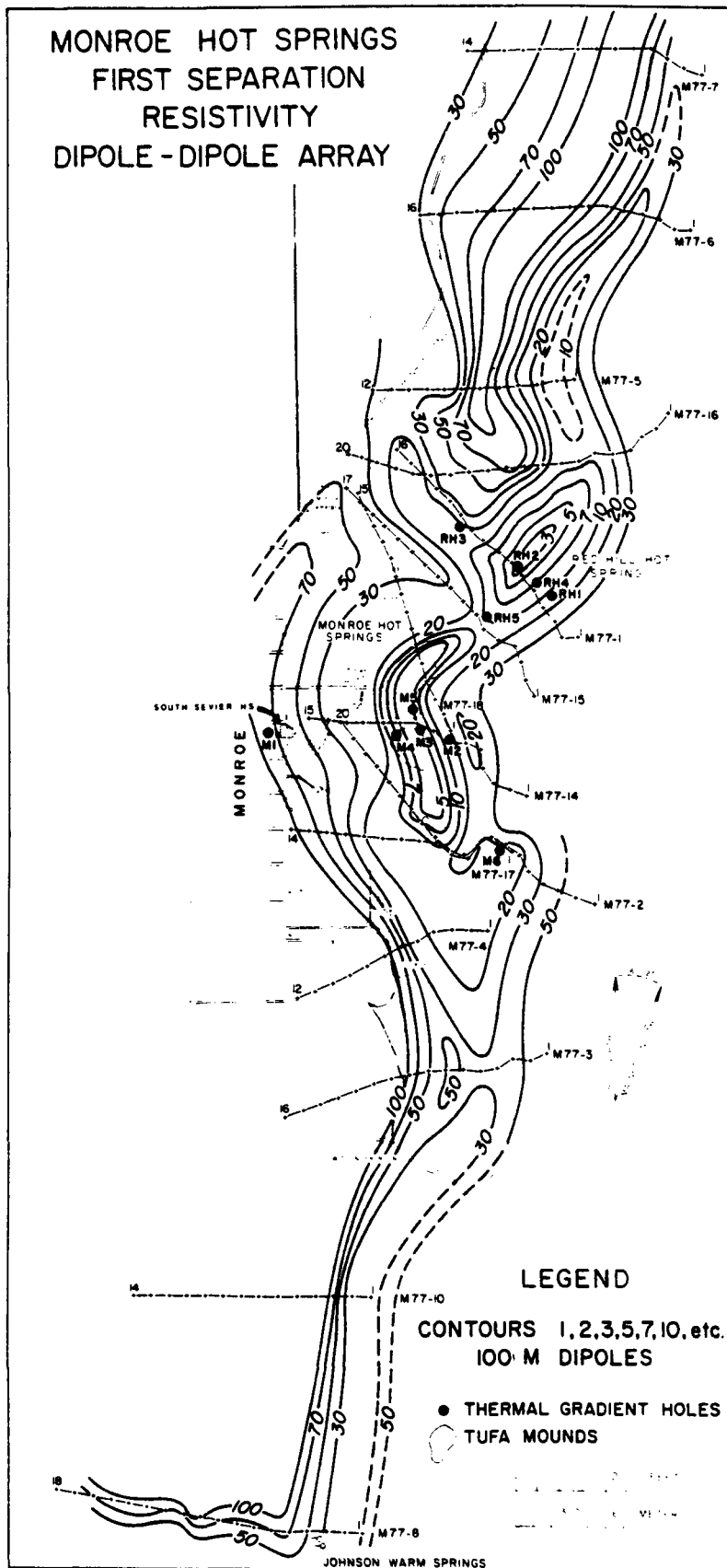
Figure 6: Dipole-dipole first separation apparent resistivity contour map of the Monroe system.

resistivity of 180 Ω-m. However this may be dramatically decreased by the intense hydrothermal alteration of the volcanics (Parry et al., 1976) and the increased fracture density caused by the Sevier fault. A similar analysis for groundwater of the central Sevier River Valley based on data from Carpenter and Young (1965) yields an apparent resistivity for the alluvium of 80-100 Ω-m. The combined sounding and profiling of a dipole-dipole resistivity survey will thus aid in detecting regions of discharge of thermal fluids from the Sevier fault zone, zones of intense hydrothermal alteration and, subsurface areas within the alluvium where thermal fluids are leaking from the system, cooling and mixing with ground water.

Fourteen resistivity profiles across the Sevier fault were used to construct a 100m dipole-dipole first separation apparent resistivity contour map, figure 6, from which inferences about the subsurface hot springs flow may be drawn. The map effectively outlines the trace of the Sevier fault and contains an elongate zone of low resistivity ($<10 \Omega$-m) associated with the discharging thermal fluids along the Sevier fault and the intense alteration accompanying the hot springs. All of the surface geothermal manifestation in the Monroe-Red Hill area are contained within the 10Ω-m contour line. This zone defines the Monroe-Red Hill system as an elongate zone .5km wide and 3km long which may consist of two plumes-one centered over the Monroe hot springs mound the other over Red Hill hot spring. The arm of low resistivity projecting northwest from Red Hill is interpreted as leakage of cooling thermal fluids through the alluvium. A similar zone is indicated extending westward from Johnson Warm

Springs.

To provide information on the subsurface geothermal regime the electrical response was modeled for lines crossing the system. The models for the Monroe mound and Red Hill are illustrated in the figures 7, 8, and 9. All models were constructed using a two-dimensional forward transmission surface algorithm to calculate theoretical dipole-dipole resistivity pseudosections for comparison with the observed pseudosections. The model pseudosection calculated for both the Monroe mound and Red Hill are reasonable matches to the observed sections. The 4 Ω-m zone on the models is interpreted to be the Sevier fault zone through which thermal fluids are being vented to the surface from the reservoir. This zone is bounded on the west by a 7 Ω-m zone in which we suspect thermal fluids leak into the alluvium. The 7Ω-m zone increases in resistivity westward to 30Ω-m which is interpreted as a zone of unsaturated alluvium. East of the fault zone is a hydrothermal alteration zone extending into the Bullion Canyon volcanics. Lines M77-16 and M77-2 located on the north and south ends of the system and M77-15 located between the hot springs indicate that the systems consist of two plumes, one located beneath the Monroe mound the other beneath the Red Hill hot springs. Resistivity models indicate that the two plumes are separate at depths to 400m although leakage and subsequent cooling may be taking place laterally along the fault zone.

To see if the electrical response was sensitive to the dip of the Sevier fault the model for Line M77-14, figure 7, was taken and the dip of the 4 Ω-m zone was allowed to decrease until the fit with the

LINE M77-14   SS CANYON
(100 M DIPOLES)
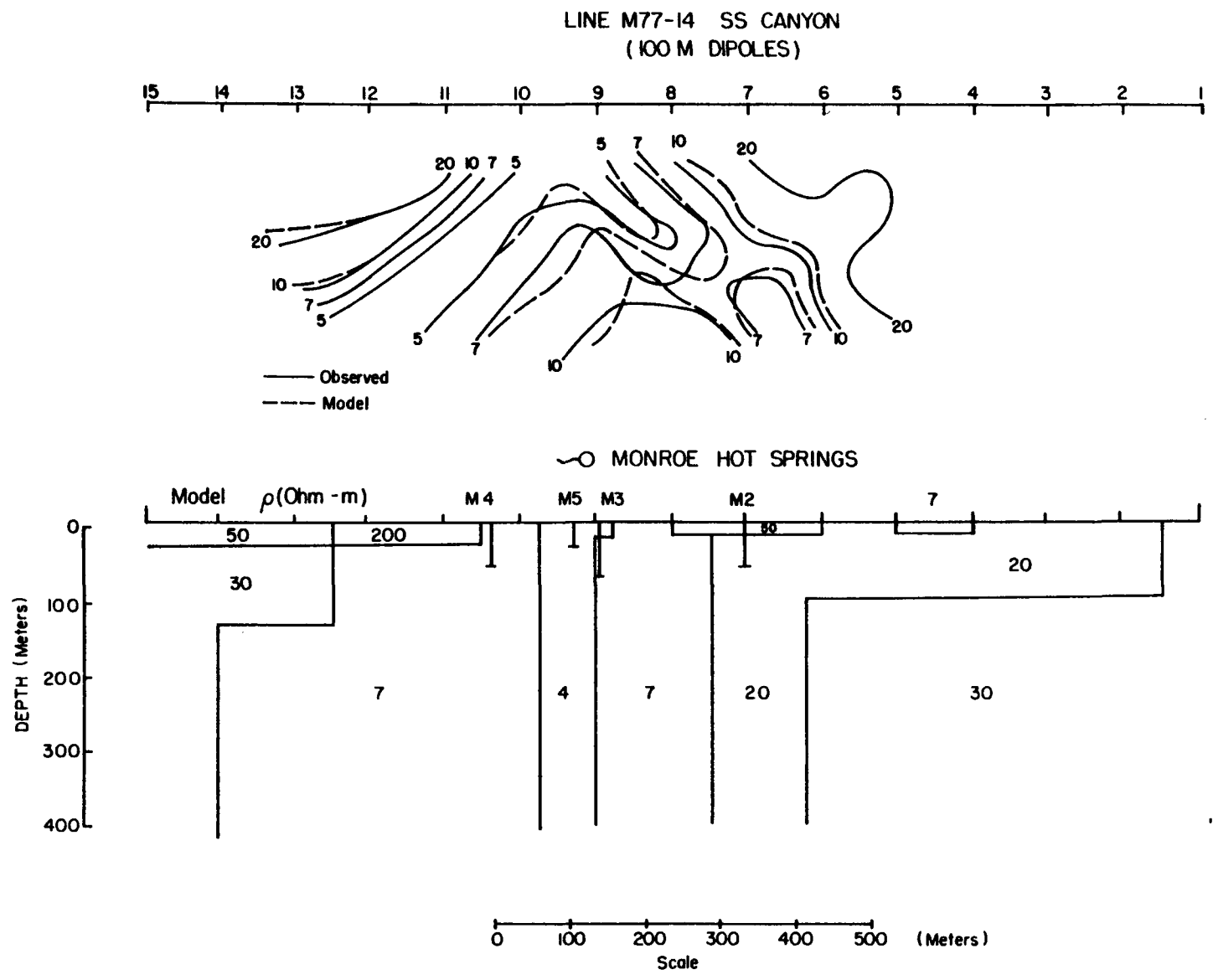
Figure 7: Electrical resistivity model, Line M77-14.
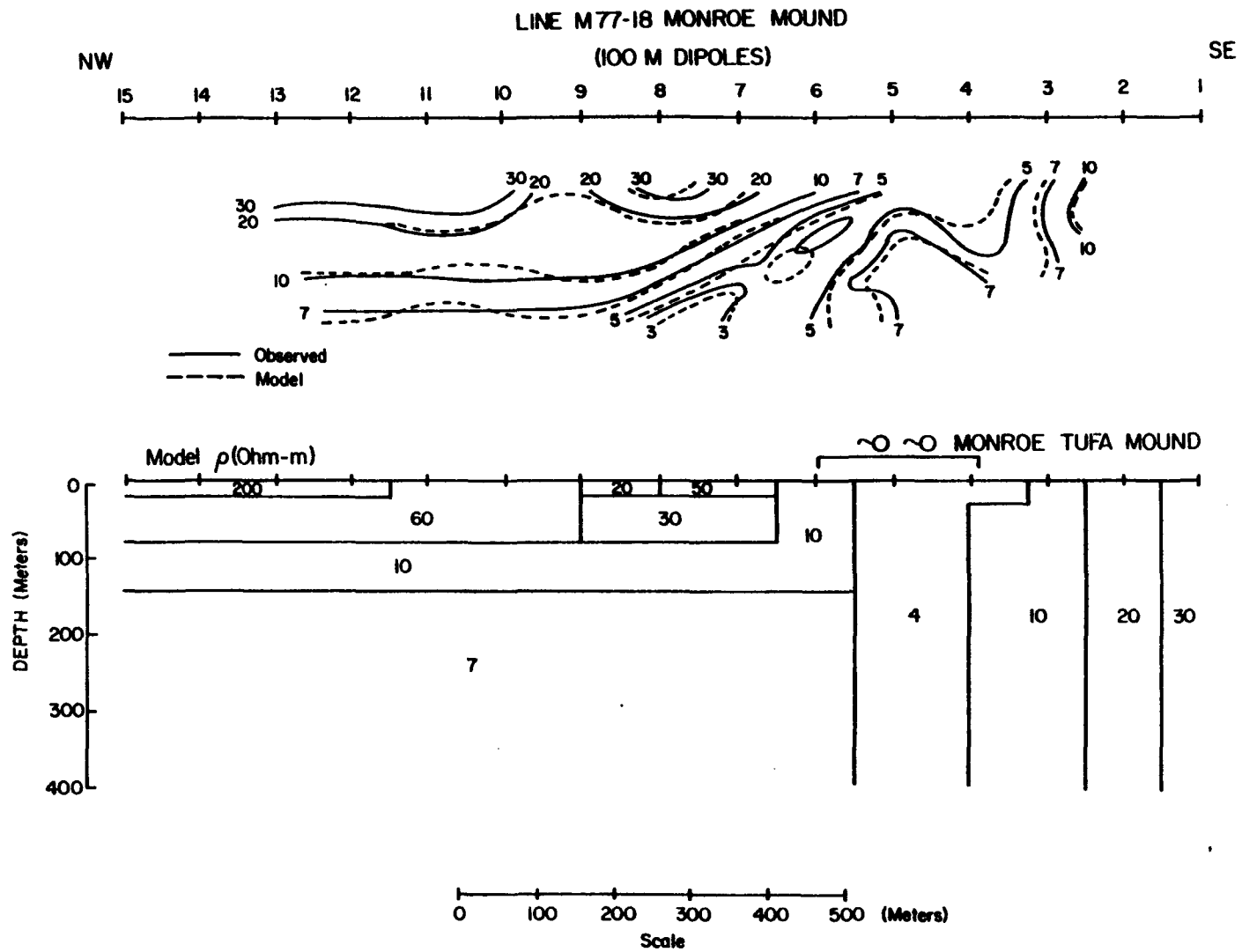
Figure 8: Electrical resistivity model, Line M77-18.

LINE M77-1 RED HILL
(100M DIPOLES)

NW   SE

16   15   14   13   12   11   10   9   8   7   6   5   4   3   2   1

20   20   10 7 5   5   7   10   20

10   20

5   7   5

——— Observed
— — — Model

RED HILL SPRING ～O

Model   (Ohm-m)   RH3   RH2   RH4   RH1

0 ⌐   50   40

20   30   10

4   10

100

25   30

200   10   7

20

300

400

0   100   200   300   400   500   (Meters)
Scale
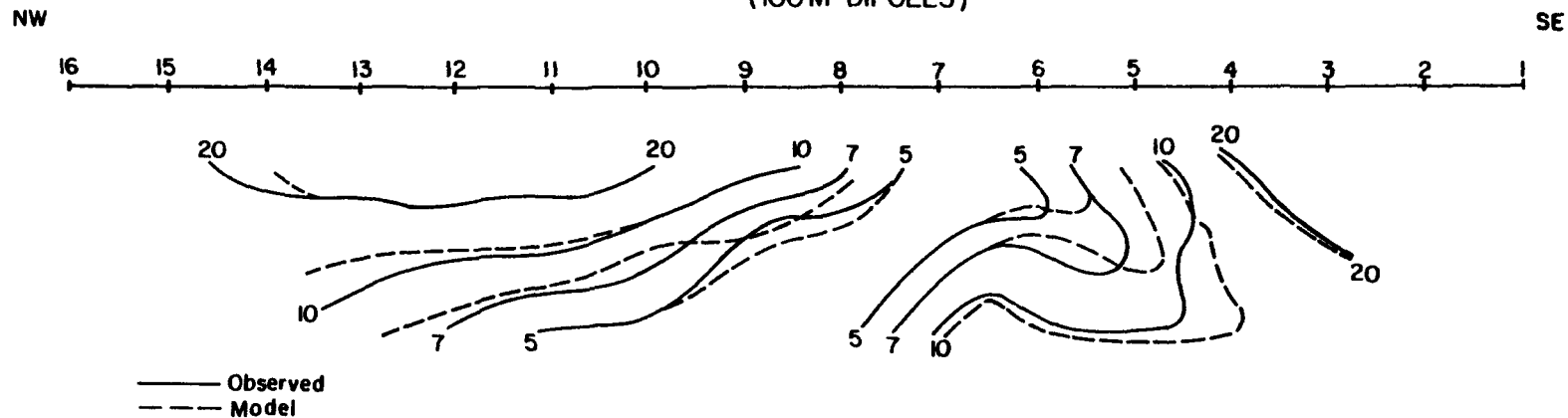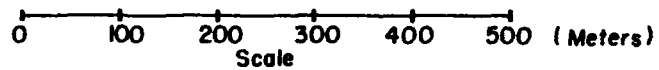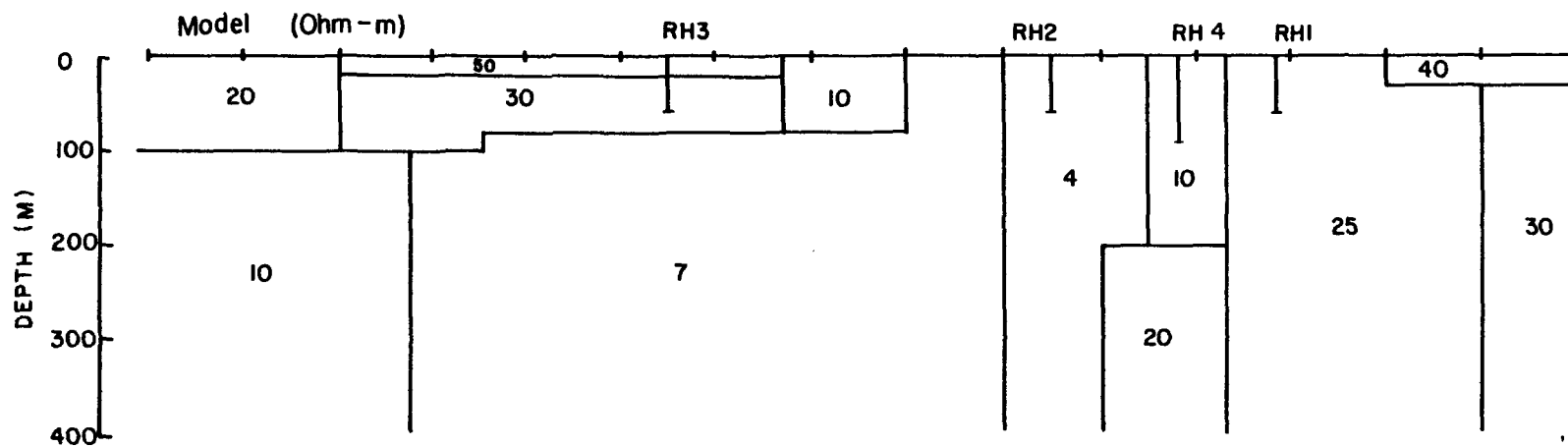
Figure 9:   Electrical resistivity model, Line M77-1.
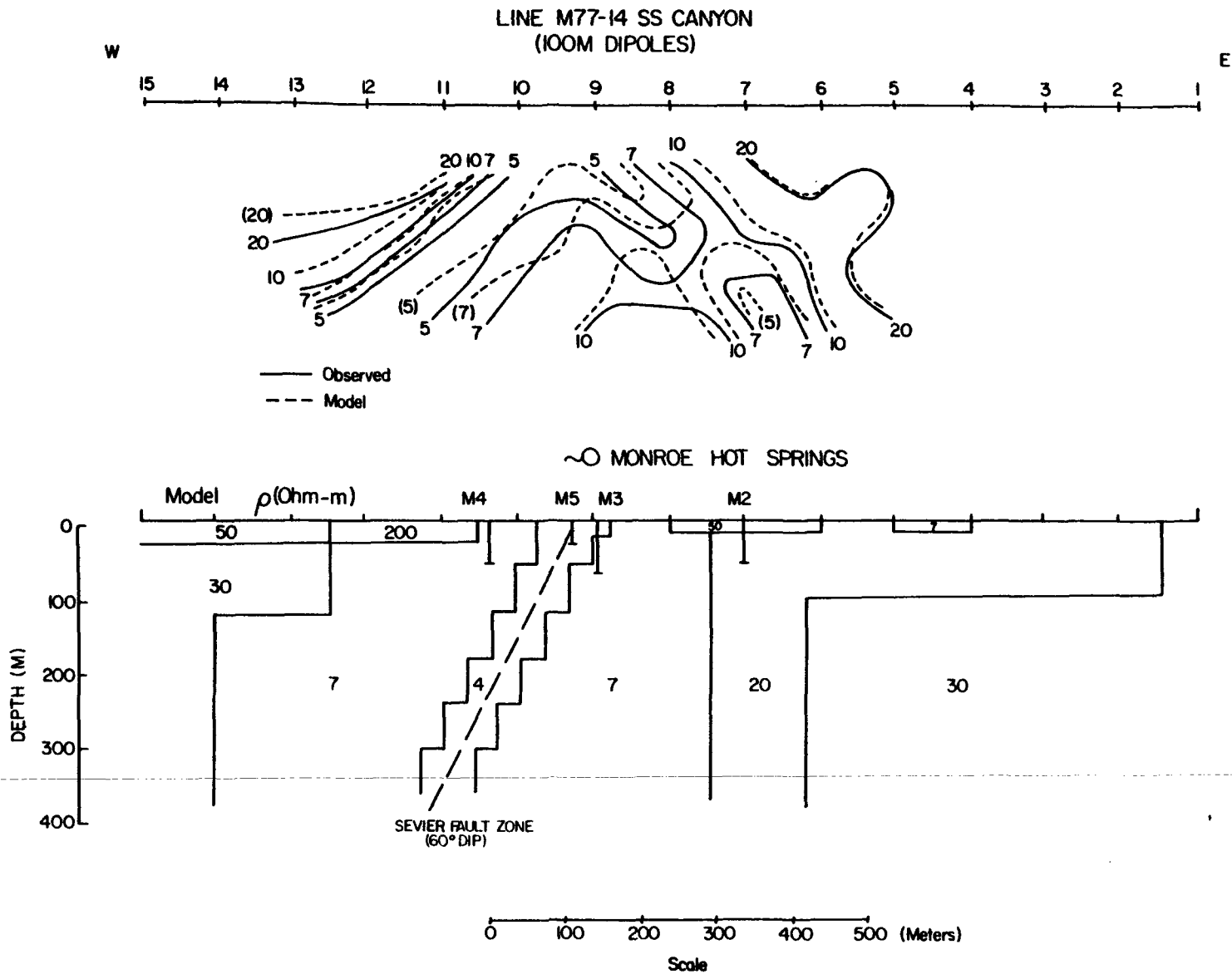
Figure 10: Electrical resistivity model, Line M77-14, with 60° dip on the Sevier fault.

observed section was observed to deteriorate. No significant deterioration was observed until a dip of 60° for the zone was used. The fit between the model and observed pseudosections shown in figure 10 has deteriorated significantly from the vertical zone of figure 7, indicating that the dip of Sevier fault zone probably lies between 70° and 90°.

To determine a minimum depth of the system a highly resistive basement was placed below the models at decreasing depths until noticable perturbations were observed on the n=4 spacing apparent resistivities. This depth was observed to be approximately 400m. As Ward and Sill (1976) have shown it is impossible to determine the depth extent of a conductive body when the body has a vertical extent that is several times its width.

Geothermal Gradient Data

The Sevier fault zone from which the hot springs issue has been adequately mapped by dipole-dipole resistivity and ground magnetics (Halliday, 1978). Furthermore, gravity studies have yielded information about the geometry of faulting through the system. The lateral and subsurface extent of the Monroe-Red Hill system has also been been inferred from dipole-dipole resistivity. Unfortunately, all these methods give us no direct information about the thermal state of the system beneath the surface. To obtain information on the thermal state at depth, a series of eleven geothermal gradient-heat flow boreholes was drilled. Ten of the boreholes comprise two profiles, one across the Monroe hot springs mound, the other across the Red Hill

hot spring. The profiles were selected to cross the two elongate zones of low resistivity (<10 Ωm) centered over the springs. Temperature measurements and detailed thermal conductivity measurements were made on each borehole to provide estimates of conductive heat flow. Unfortunately, detailed hydrologic measurements needed to calculate local mass fluxes in the convective system were not undertaken.

A peculiarity of temperature-depth curves near strongly convecting zones is that the thermal gradient is large and quite variable with depth, so that making temperature extrapolations on the basis of these curves is risky. Figure 11 illustrates temperature depth curves for the Monroe hot springs profile. The location of the boreholes is indicated in figure 6, their relationship to the Sevier fault and Monroe tufa mounds is shown in the inset. M6 has a nearly constant geothermal gradient of 240°C km^{-1}, while the remaining four boreholes (M2, M3, M4, and M5) all show a strong, consistent, downward curvature. This curvature could indicate an increase of thermal conductivity with depth, lateral heat conduction away from a strongly convecting system, or a weak, diffused, upward convection. As detailed thermal conductivity measurements at 5 m intervals indicate no increase in thermal conductivity with depth, the cause of the curvature is likely either lateral heat conduction or diffused upward convection. The increase in degree of curvature as the Sevier fault is approached suggests that the fault is the locus of the convecting system.

An isotherm cross section of the Sevier fault has been created by

TEMPERATURE (°C)

DISTANCE (m)
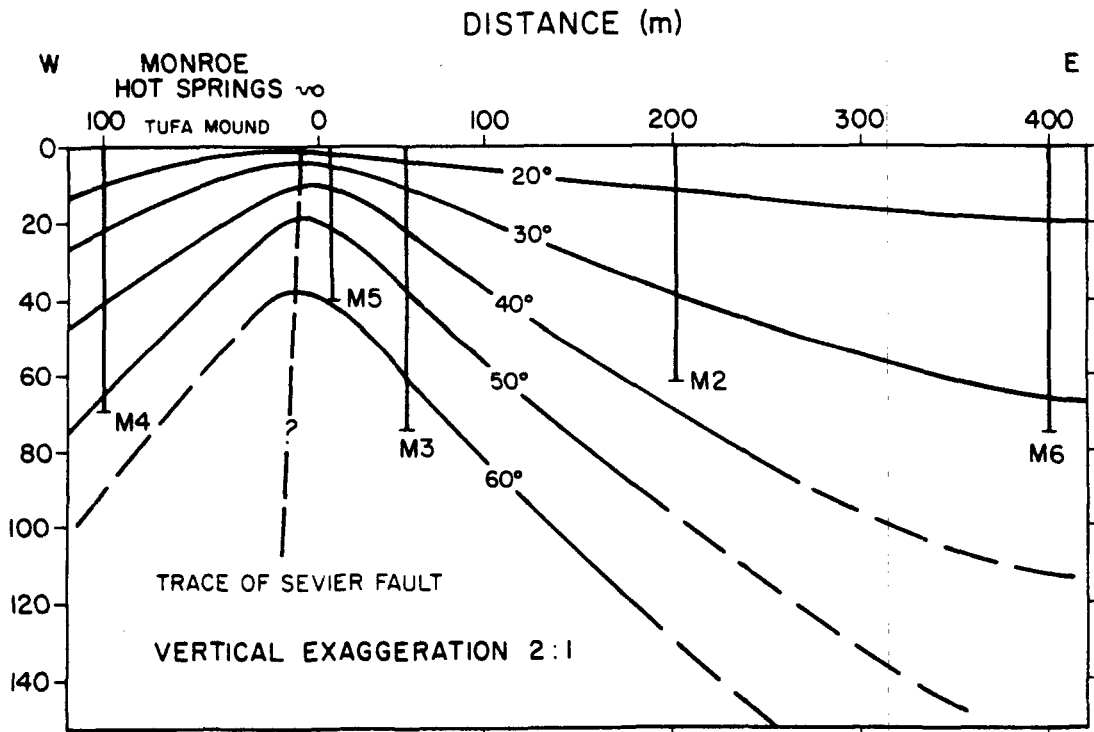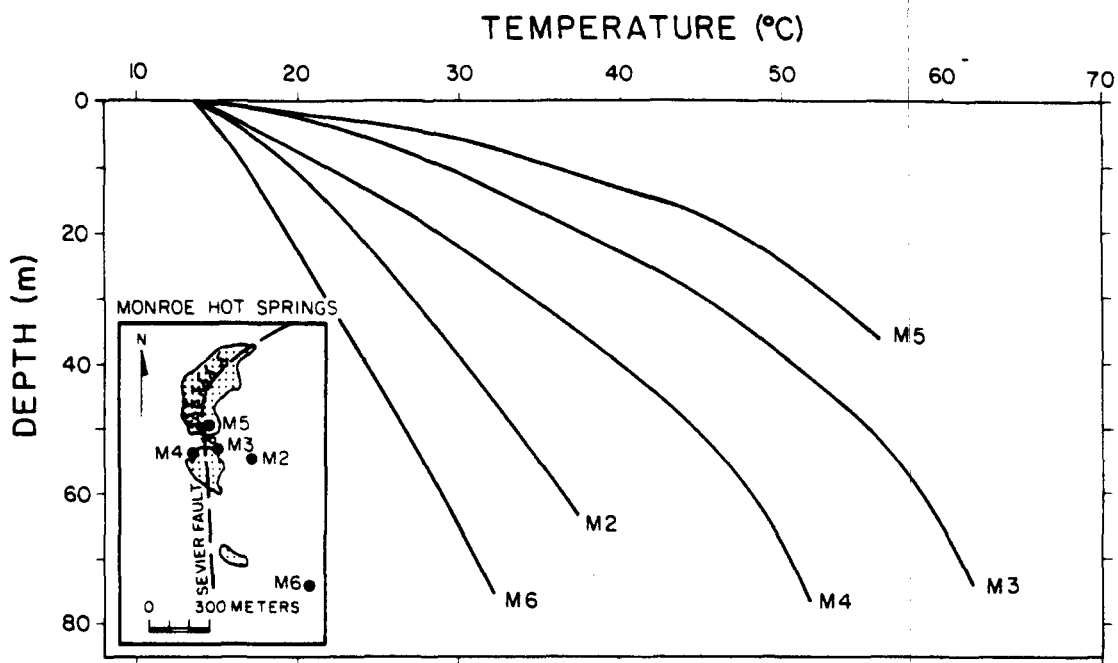
Figure 11: Temperature-depth curves and isotherm cross section for Monroe hot springs.
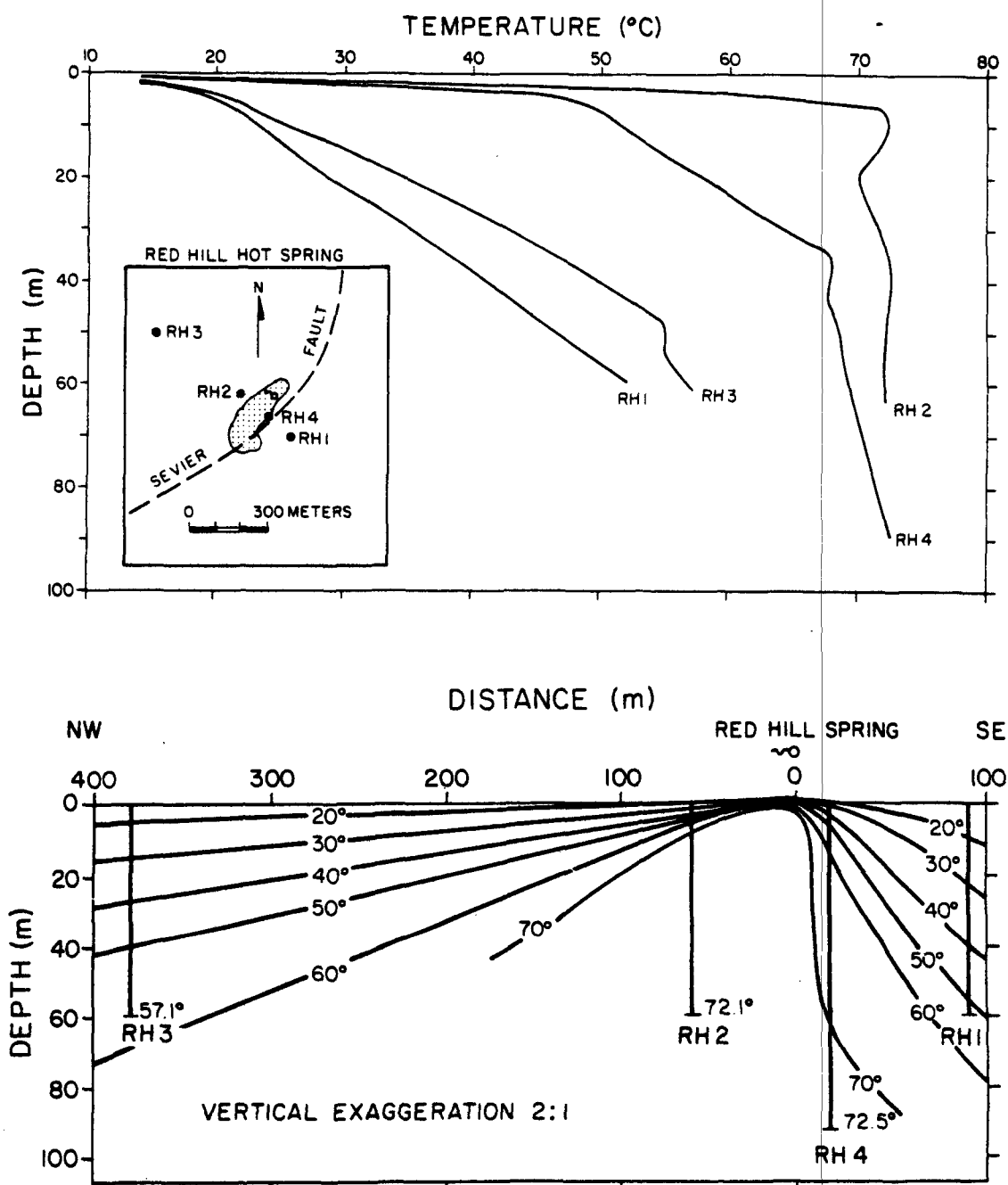
Figure 12: Temperature-depth curves and isotherm cross section for Red Hill hot springs.

projecting the borehole temperature data at Monroe on to a east-west line perpendicular to surface trace of the Sevier fault (Fig. 12). The isotherms are upwarped under the discharge vent and taper off to the east and west. The upwarping of the isotherms is qualitatively similar to the pattern produced in the numerical models of Blackwell and Chapman (1977) for thermal fluids of constant temperature circulating up a dipping plane. Kilty et al. (1978) have also simulated such a thermal regime by numerically modeling forced convection through a fault zone with little leakage into the alluvium.

Temperature-depth curves for the Red Hill profile are shown in figure 12 with drill hole locations shown in the inset. The nearly isothermal appearance of two of the boreholes at Red Hill indicates a strongly convecting system beneath a conductive cap. The near isothermal nature of these boreholes will probably continue until a zone of mixing with cooler ground water occurs where the temperature may increase $10-15^{\circ}C$ and then continue isothermally to the hot reservoir (Kilty et al., 1978). The remaining two boreholes, RH1 and RH3 yield reasonably constant gradients of 580 $^{\circ}C$ km^{-1} and 780 $^{\circ}C$ km^{-1} respectively. The location of RH2 was selected so that it would lie within the low resistivity zone extending northwestward from Red Hill, which is believed to be associated with the leakage of thermal fluids westward into the alluvium. The isothermal character of RH2 at 50 m depth is interpreted as indicating movement of thermal fluids within alluvial gravels at that depth.

A northwest-southeast isotherm cross section of the temperature data at Red Hill is also displayed in figure 12. The isotherms are

upwarped under the discharge vent and taper off to the east and west. The pronounced asymmetry in the isotherms may be attributed to several effects: (1) leakage of thermal fluids westward into the alluvium, (2) the dip of the fault zone through which the thermal fluids are rising, and (3) lower thermal conductivity of the alluvium to the west of the fault in contrast to the volcanics to the east. Since gravity models and models by Kilty et al. (1978) depict the fault to be steeply dipping, the effects of dip should be small. The thermal conductivity contrast between alluvium (1.7 W m^{-1} K^{-1}) and volcanics, (2.3 W m^{-1} K^{-1}) would explain some of the observed asymmetry but the leakage hypothesis is preferred (Kilty et al., 1978).

Heat Flow

The vertical component of heat flow was computed as the product of the measured thermal conductivity and the vertical temperature gradient. Thermal conductivities were measured on solid discs of core or from drill chips in a divided bar apparatus following the methods described by Sass et al. (1971a, 1971b). Assigning a single gradient in drillholes exhibiting curvature in the temperature-depth plot for the purpose of calculating a conductive heat loss is somewhat arbitrary. In general the most linear section of the near surface temperature-depth curve was used to calculate the least squares gradient. Table 1 gives results for each hole including the depth interval and corresponding gradient, mean thermal conductivity, and heat flow. The heat flow varies from 548 mW m^{-2} in drillhole M6 which is furthest from the active system to more than 3400 mW m^{-2} in RH2.

Table 1
Thermal Gradient, Conductivity and Heat Flow

Drillhole	Depth Range (m)	Gradient (^oC km^{-1})	N	Conductivity (W m^{-1} K)	Heat flow (mW m^{-2})	Apparent resistivity (Ω-m)
M1	-	-	-	-	-	-
M2	10-61	336(4)	11	2.31(.13)	775(7)	16
M3	10-72	725(16)	14	2.33(.21)	1689(25)	5
M4	10-40	615(17)	11	1.76(.23)	1082(23)	7
M5	10-38	739(31)	5	2.52(.37)	1836(50)	4
M6	10-75	238(2)	14	2.30(.24)	548(5)	23
RH1	10-60	591(2)	11	2.52(.24)	1488(7)	10
RH2	0-08	7200(950)	9	.47(.26)*	3400(650)	3
RH3	10-48	778(10)	9	1.49(.23)	1160(14)	16
RH4	0-06	5400(710)	15	.62(.34)**	3350(560)	8
RH5	10-46	628(4)	7	1.38(.10)	866(5)	12

* 1.58(.35) for water saturated alluvium

   .47(.26) for air saturated alluvium

** 2.14(.19) for water saturated alluvium

   .62(.34) for air saturated alluvium

All values are considerably enhanced over a background regional heat flow of 75-100 mW m^{-2} which is typical of Basin and Range heat flow in Utah.

The variation of heat flow across a geothermal system can be diagnostic of the subsurface thermal and fluid flow regime. Two heat flow profiles for this system, one crossing the Monroe mound and the other crossing the Red Hill mound are shown in Fig. 13. Whereas both profiles have similar trends of decreasing heat flow to the east, the western limbs of the profiles are markedly different. The difference is consistent with a more pronounced leakage of warm thermal fluids in the alluvium west of Red Hill inferred previously from the electrical resistivity data.

In spite of the limited spatial coverage provided by the eleven heat flow determinations, a heat flow map of the area has been constructed (Fig. 14). In regions where no heat flow drill holes exist the contouring is controlled on the basis of the apparent resistivity map and an empirical relationship between heat flow and resistivity. The heat flow at a drill site and the apparent resistivity deduced from the first separation 100 m dipole-dipole survey (Table 1) are related as follows:

$$q = 5800 \, \rho_a^{-.706}$$

The correlation (shown in the inset of Fig. 14) may be attributed to the cooling and mixing of the hot spring waters as they discharge and move away from the fault resulting in an increase in apparent resistivity and a decrease in conductive heat flux. Accompanying this
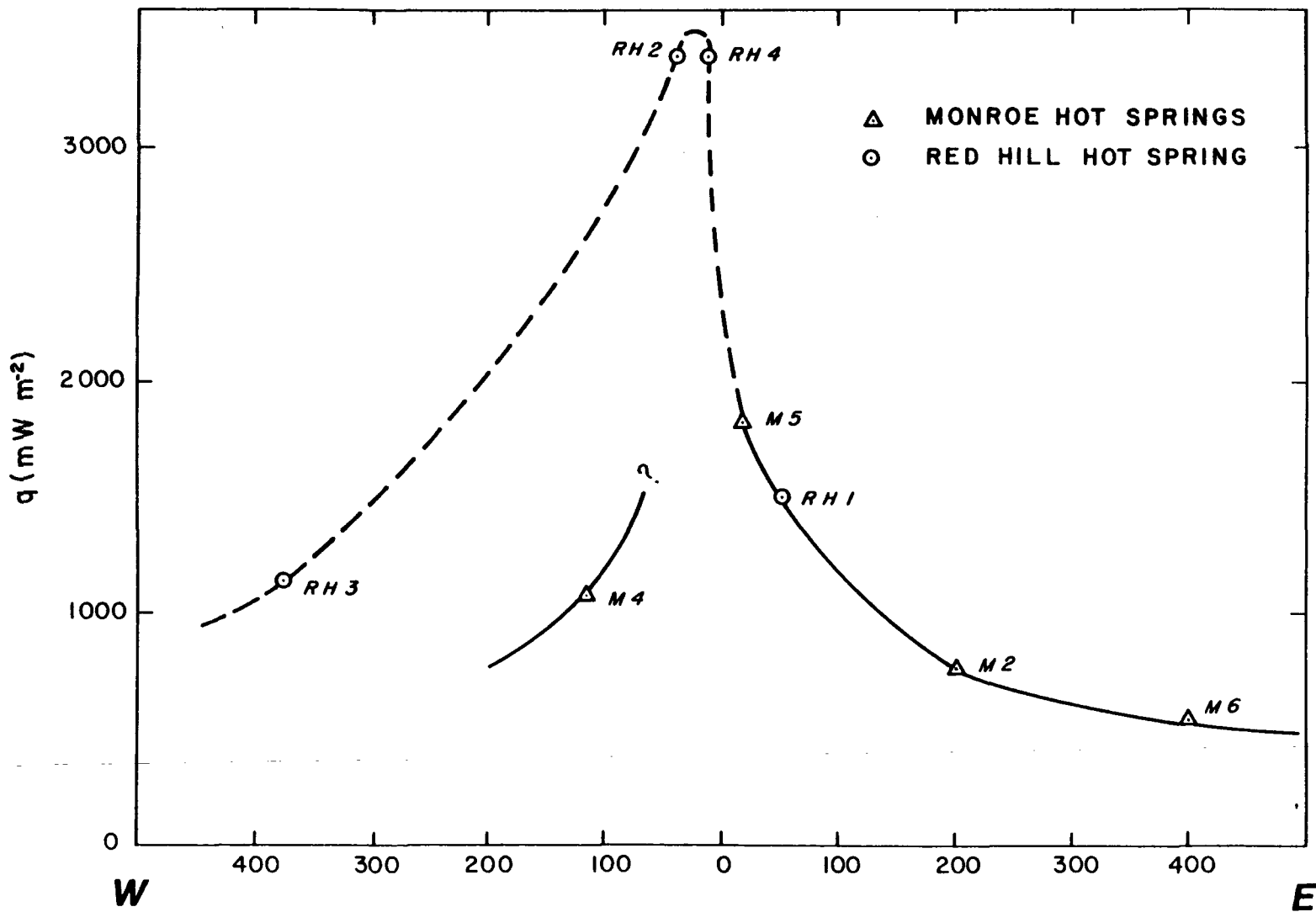
Figure 13: Heat flow profiles.

MONROE – RED HILL HEAT FLOW
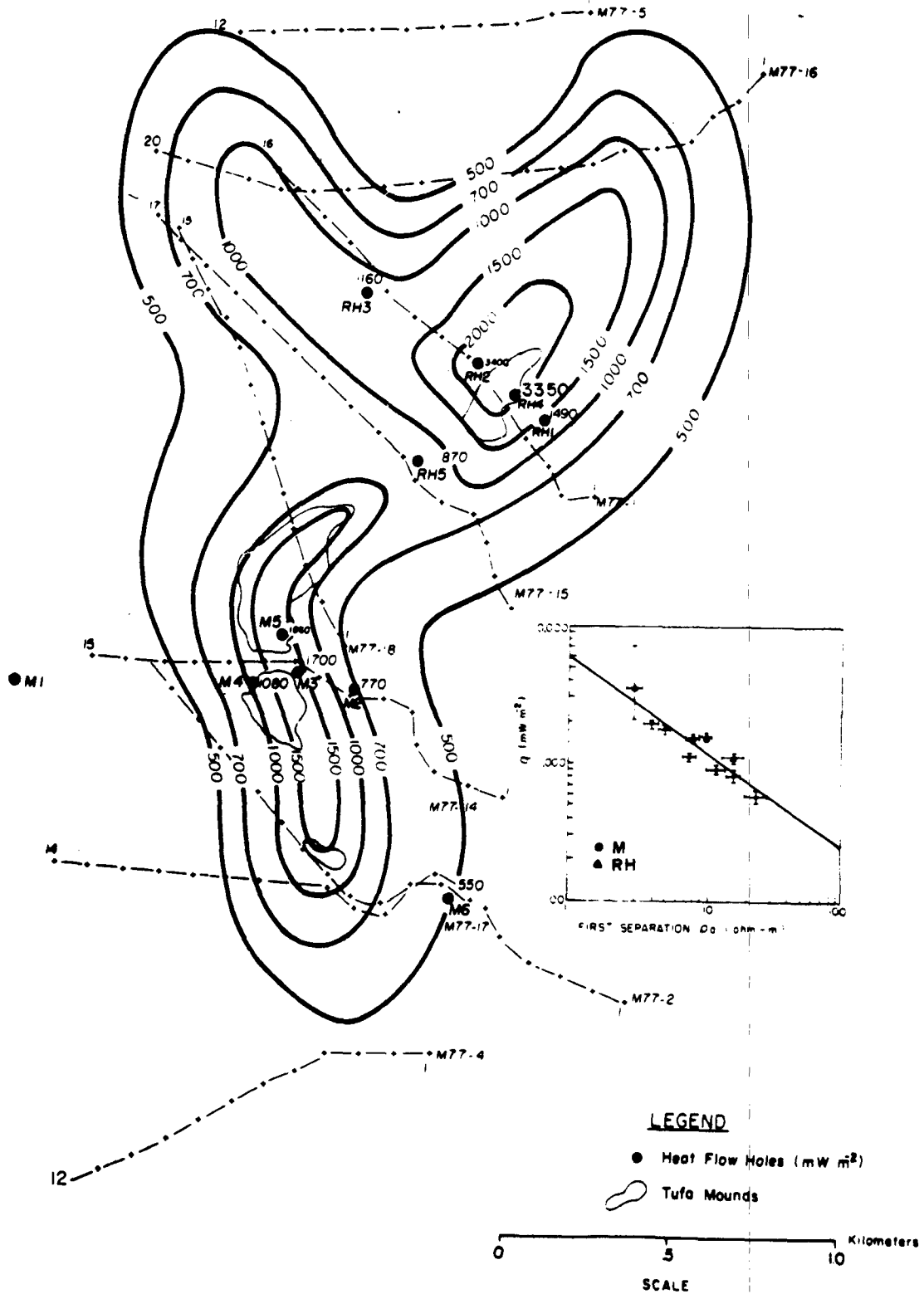
Figure 14: Monroe-Red Hill heat flow map.

is a decrease in alteration products (clays) away from the system
resulting in an increase in resistivity. The heat flow contours
outline the surface geothermal manifestations and indicate that the system
is composed of two-pipe like conduits contained within the fault zone,
through which thermal fluids are being discharged. A zone of leakage
is indicated, extending northwestward from the system.

The total power loss at Monroe-Red Hill can now be estimated by
integrating the heat flow over the system and adding to this the
enthalpy of the water. From figure 14 the conductive heat loss inside
the 500 mW m^{-2} contour is estimated at 2.9 MW. The discharge at Red
Hill spring is 12.8 liters per second at a temperature of 75°C and the
combined discharge of all the seeps at Monroe Hot Spring is 5.8 liters
per second at a maximum temperature of 70°C. This yields a convective
power loss of 4.9 MW. The net heat discharge from the Monroe-Red Hill
system is thus 7.8 MW. This is equivalent to the normal Basin and
Range heat flow over a 100 km^2 area. Figure 15, shows the percentage
of normal Basin and Range heat flow over a given area required to
supply the estimated power loss at Monroe-Red Hill. If recharging
groundwater absorbs 30 to 50% of the regional heat flow as is the case
in the Roosevelt Hot Springs region (Wilson and Chapman, 1978), heat
absorbed over a recharge area of 200 to 350 km^2 could maintain the
observed power loss at Monroe-Red Hill. The Sevier Plateau to the
east and south of hot springs contains approximately 1000 km^2 of
possible recharge area. The ground water may also absorb a substantial
amount of heat in lateral movement to the hot storage reservoir.
Unfortunately, no heat flow measurements are available away from the
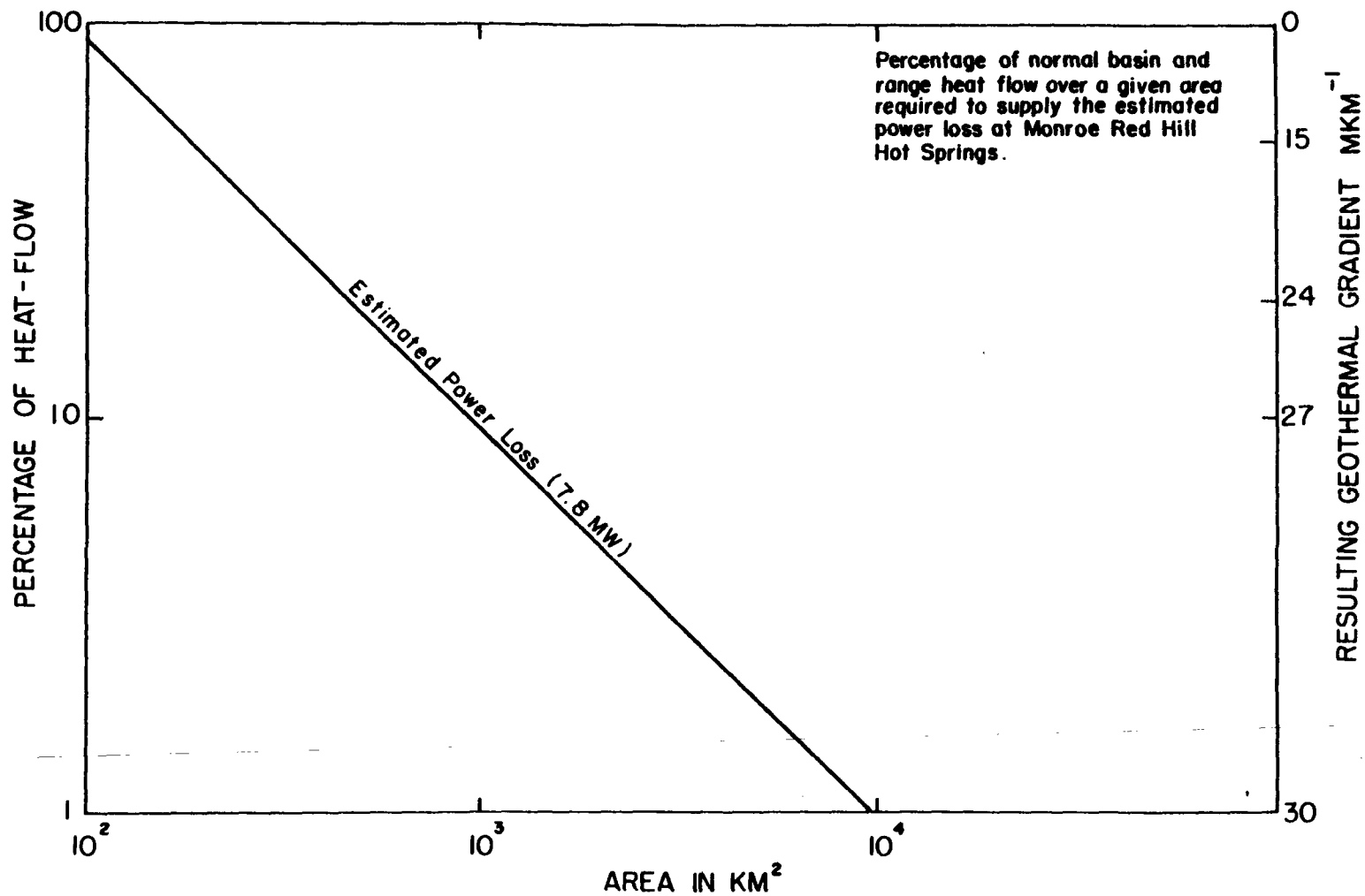
Figure 15: Percentage of normal Basin and Range heat flow over a given area required to supply the estimated power loss for the Monroe-Red Hill system.

immediate area around the hot spring. Such data would provide useful information on the location of the recharge area and subsurface groundwater flow (Lachenbruch et al., 1976).

CONCLUDING REMARKS

The geological, geochemical, and geophysical data collected at
Monroe constitute a compatible set. Each member of the set (i.e. geo-
chemistry, heat-flow, resistivity, gravity, and ground magnetics) has
been interpreted separately to obtain estimates of the system's confi-
guration. Each of these interpretations also serves to substantiate
the interpretation of the other data set. This type of analysis re-
sults in a pooled, hence more reliable, interpretation of the Monroe
geothermal system.

The system is aligned north-south along the prominent Sevier fault
zone. A dip of 80° ± 10° for the Sevier fault satisfies the gravity,
resistivity and heat flow data sets. The geometry of the fault zone
is likely a complexly fractured zone.

Hot and warm springs occur at changes in the surface trace of the
Sevier fault. Perhaps these are the only places where permeable con-
duits exist in the fault zone through which water may rise to the
surface. Conceivably hot water may come from depth in many other places
along the fault zone, only to mix with cool water and leak into the
alluvium before it can be discharged at the surface. The discharge
pattern for the hydrothermal system is revealed by the resistivity and
heat flow surveys.

A maximum temperature of 74°C was measured in borehole RH2 at Red
Hill. The nearly isothermal behavior of two of the boreholes at Red
Hill will probably continue until a zone of cold water mixing is reached.
The temperature could increase from 10-15°C through the mixing zone and

continue isothermally to the hot reservoir. A reservoir temperature of 118°C was predicted from geothermometry but the depth at which this temperature might be achieved depends on levels of cold water mixing in the system. The thermal structure can be effectively modeled by assuming discharge of hot water from a reservoir at depth upward through the Sevier fault zone.

The net heat discharge from the Monroe-Red Hill system is 7.8 MW based on conductive and convective heat loss. Heat transfer by moving ground water in a normal Basin and Range heat flow environment can easily provide the observed power loss. There is no need for additional exotic heat sources such as a cooling magma chamber.

The conceptual model of a fault controlled hydrothermal system documented by this study provides a detailed rationale for further exploration and eventual development of this system.

APPENDIX I

Ground Magnetics: Data Acquisition and Reduction

A total of 840 ground magnetic stations was established along 19
profiles in a 40 km^2 area along the Sevier fault. A complete listing
of these values plus a description of the magnetic base may be
obtained in Halliday (1978). These profiles follow the dipole-dipole
resistivity lines except in the Monroe-Red Hill area where detailed
lines were included. A standard looping technique was used to collect
the data with loops being closed twice daily back to a magnetic base
station. Station spacing was 20m in the vicinity of the hot springs
and 50m for lines on the peripherals. Readings were taken in a star
pattern, one reading being taken at the center with four additional
readings at 3 m from the station at the principal compass points. The
readings were then averaged to reduce high frequency noise associated
with a volcanic terrain. Diurnally corrected values were then
calculated assuming a linear drift between values taken at the base
station. Total magnetic intensity anomalies were then determined by
subtracting the total magnetic field at the base station. Therefore,
all anomaly values are referenced to the magnetic base station.

Measurements of the total magnetic field were made using a
Geometrics model G816 proton precession magnetometer. The precision
this device is 1 gamma. Repeated measurements were made for selected
stations to determine the accuracy of the measurements. Average
differences were found to be within 10 gammas, a reasonable estimate

of the error residing in each total magnetic intensity anomaly value.
A three-wire power transmission line that extends north-south through
the survey area caused magnetic noise. These readings were easily
recognized near the power line by their erratic nature and dropped off
rapidly away from the line so as to be negligible. No readings were
taken adjacent to or underneath the power line. The drift of the
proton precession magnetometer is considered to be negligible and no
corrections have been applied to remove the earth's magnetic field
gradient because of the small areal extent of the survey.

As an aid in interpretation of the total magnetic intensity
anomaly map magnetic susceptibilities were made on the core and chip
samples from the thermal gradient-heat flow drilling. Measurements
were made on a Geophysical Specialties model MS-2 magnetic
susceptibility bridge. No repeat measurements were made on the
samples to estimate a standard error residing within each value.
Table 1 contains a summary of magnetic susceptibility measurements
with average susceptibility and standard deviation for major rock
types.

Heat flow hole	Depth below surface (m)	Rock type	Magnetic Susceptibility (c.g.s. units)
M1	6	alluvium	.0013
M1	30	alluvium	.0012
M1	61	alluvium	.0024
M1	91	alluvium	.0026
M2	9	Tbc (latite)	.0001
M2	30	Tbc (latite)	.0006
M2	61	Tbc (latite)	.0002
M3	14	Tbc (agglomerate)	.0001
M3	50	Tbc (agglomerate)	.0005
M3	75	Tbc (agglomerate)	.0003
M4	6	alluvium	.0006
M4	37	alluvium	.0005
M4	73	alluvium	.0003
M5	--	Tbc (latite)	.0001
M6	20	Tbc (latite)	.0001
M6	65	Tbc (latite)	.0000
RH1	6	alluvium	.0000
RH1	12	Tbc (agglomerate)	.0001
RH1	18	Tbc (agglomerate)	.0000
RH1	30	Tbc (agglomerate)	.0000
RH1	46	Tbc (agglomerate)	.0000
RH1	61	Tbc (agglomerate)	.0000
RH2	6	alluvium	.0011
RH2	12	alluvium	.0013
RH2	31	alluvium	.0012
RH2	46	alluvium	.0009
RH2	61	alluvium	.0010
RH3	6	alluvium	.0011
RH3	31	alluvium	.0016
RH3	61	alluvium	.0017
RH4	6	alluvium	.0000
RH4	31	alluvium	.0003
RH4	61	alluvium	.0001
RH4	91	alluvium	.0002
RH5	6	alluvium	.0012
RH5	31	alluvium	.0024
RH5	61	Tbc (latite)	.0003
RH5	73	Tbc (latite)	.0004
outcrop	surface	Tbc (latite)	.0005
outcrop	surface	Tbc (latite)	.0003
outcrop	surface	Tbc (basaltic andesite)	.0042
outcrop	surface	Tbc (basaltic andesite)	.0026

$\overline{\mu}$Tbc (latite and agglomerate) = .0002 $\sigma_{\overline{\mu}}$ = .0002

$\overline{\mu}$alluvium = .0015 σ_{μ} = .0006

$\overline{\mu}$alluvium adjacent to hot springs = .0002 $\sigma_{\frac{\mu}{\mu}}$ = .0002

APPENDIX II

Gravity Data

The elevation and free air anomaly for the stations comprising the Monroe-Red Hill profile were obtained from Halliday (1978). Details as to their exact location and method of data acquisition has been described by him. The covariance between elevation and Bouguer values was calculated for densities ranging from 1.7 to 2.8 gm cm^{-3}, table 2, and a minimum value for a density of 2.5 gm cm^{-3} was obtained. This value was used to reduce the free air to a simple Bouguer. Terrain corrections for a density of 2.67 gm cm^{-3} have been calculated for each station by Halliday (1978). These values were taken and amended to yield a terrain correction value for 2.50 gm cm^{-3} which was used in computing the complete Bouguer. Table 3 lists station identification, elevation, free air anomaly, simple Bouguer, terrain correction and complete Bouguer for each station. Errors in the gravity value due to vertical control, tidal effects, and instruments were estimated by Halliday (1978) to be less than 1 mgal. The major error resides in the terrain correction and can be estimated by taking 10% of the terrain correction value.

COVARIANCE ANALYSIS-ELEVATION AND BOUGUER GRAVITY

STATION	ELEVATION (METERS)	BOUGUER GRAVITY AT DIFFERENT DENSITIES										FREE AIR
		1.8	1.9	2.0	2.1	2.2	2.3	2.4	2.5	2.6	2.7	
MH615	3402.	-121.7	-135.9	-150.2	-164.5	-178.7	-193.0	-207.2	-221.5	-235.7	-250.0	135.0
MH514	3422.	-127.2	-141.5	-155.8	-170.2	-184.5	-198.9	-213.2	-227.6	-241.9	-256.2	131.0
MH077	2750.	-136.9	-148.4	-159.9	-171.5	-183.0	-194.5	-206.0	-217.6	-229.1	-240.6	70.6
MH076	2787.	-142.9	-154.5	-166.2	-177.9	-189.6	-201.3	-212.9	-224.6	-236.3	-248.0	67.4
MH075	2669.	-144.3	-155.5	-166.7	-177.9	-189.1	-200.2	-211.4	-222.6	-233.8	-245.0	57.0
MH079	2352.	-146.0	-155.9	-165.7	-175.6	-185.5	-195.3	-205.2	-215.0	-224.9	-234.7	31.4
RH010	1764.	-164.2	-171.6	-179.0	-186.4	-193.8	-201.2	-208.6	-216.0	-223.4	-230.8	-31.1
RH020	1748.	-164.6	-171.9	-179.2	-186.6	-193.9	-201.2	-208.5	-215.9	-223.2	-230.5	-32.7
RH030	1745.	-164.5	-171.8	-179.2	-186.5	-193.8	-201.1	-208.4	-215.7	-223.0	-230.4	-32.8
RH040	1720.	-166.0	-173.2	-180.5	-187.7	-194.9	-202.1	-209.3	-216.5	-223.7	-230.9	-36.3
RH050	1711.	-166.9	-174.1	-181.3	-188.4	-195.6	-202.8	-210.0	-217.1	-224.3	-231.5	-37.9
RH060	1704.	-168.1	-175.2	-182.4	-189.5	-196.7	-203.8	-210.9	-218.1	-225.2	-232.4	-39.6
RH070	1691.	-169.2	-176.3	-183.3	-190.4	-197.5	-204.6	-211.7	-218.8	-225.9	-233.0	-41.6
RH080	1684.	-169.9	-176.9	-184.0	-191.1	-198.1	-205.2	-212.2	-219.3	-226.3	-233.4	-42.8
RH090	1675.	-170.7	-177.7	-184.7	-191.7	-198.8	-205.8	-212.8	-219.8	-226.8	-233.9	-44.3
RH100	1669.	-171.4	-178.4	-185.4	-192.4	-199.4	-206.4	-213.4	-220.4	-227.4	-234.3	-45.5
RH110	1663.	-172.1	-179.0	-186.0	-193.0	-199.9	-206.9	-213.9	-220.8	-227.8	-234.8	-46.6
RH120	1657.	-172.7	-179.7	-186.6	-193.6	-200.5	-207.5	-214.4	-221.3	-228.3	-235.2	-47.7
RH130	1653.	-173.4	-180.3	-187.3	-194.2	-201.1	-208.0	-215.0	-221.9	-228.8	-235.7	-48.7
RH140	1647.	-174.1	-181.0	-187.9	-194.8	-201.7	-208.6	-215.5	-222.5	-229.4	-236.3	-49.9
RH150	1643.	-174.9	-181.8	-188.7	-195.6	-202.4	-209.3	-216.2	-223.1	-230.0	-236.9	-50.9
RH160	1639.	-176.3	-183.2	-190.0	-196.9	-203.8	-210.6	-217.5	-224.4	-231.2	-238.1	-52.7
RH170	1634.	-176.5	-183.4	-190.2	-197.1	-203.9	-210.8	-217.6	-224.5	-231.3	-238.2	-53.2
RH180	1631.	-177.4	-184.2	-191.0	-197.9	-204.7	-211.5	-218.4	-225.2	-232.0	-236.9	-54.3
MH009	1621.	-181.5	-188.3	-195.1	-201.9	-208.7	-215.5	-222.3	-229.0	-235.6	-242.6	-59.2
MH154	1622.	-183.6	-190.4	-197.2	-204.0	-210.8	-217.6	-224.4	-231.2	-238.0	-244.8	-61.2
MH151	1624.	-185.0	-191.8	-198.6	-205.4	-212.2	-219.0	-225.8	-232.6	-239.4	-246.5	-62.5
MH148	1638.	-186.3	-193.2	-200.1	-206.9	-213.8	-220.7	-227.5	-234.4	-241.3	-248.1	-62.8
MH170	1630.	-185.2	-192.0	-198.9	-205.7	-212.5	-219.3	-226.2	-233.0	-239.8	-246.7	-62.2
MH171	1631.	-185.1	-191.9	-198.8	-205.6	-212.4	-219.3	-226.1	-232.9	-239.8	-246.6	-62.1

| MEAN VALUE | 1914. | -166.6 | -174.6 | -182.7 | -190.7 | -198.7 | -206.7 | -214.8 | -222.8 | -230.8 | -238.8 | |

		1.8	1.9	2.0	2.1	2.2	2.3	2.4	2.5	2.6	2.7
VARIANCE	.273+06	.283+03	.218+03	.163+03	.118+03	.820+02	.557+02	.391+02	.321+02	.347+02	.469+02
COVARIANCE		.828+04	.714+04	.599+04	.485+04	.370+04	.256+04	.141+04	.265+03	-.881+03	-.203+04
CORRELATION		.9420	.9242	.8972	.8542	.7820	.6548	.4313	.0893	-.2852	-.5662

Table 3: Covariance Analysis - Elevation and Bouguer Gravity.

Table 4: Gravity Data

Station	Elevation	Free Air	Simple Bouguer	Terrain Correction	Complete Bouguer
MH615	3402.00	134.95	-221.5	22.27	-199.2
MH614	3422.00	130.98	-227.6	28.96	-198.6
MH077	2750.00	70.57	-217.6	17.34	-200.3
MH076	2787.00	67.38	-224.6	22.92	-201.7
MH-75	2669.00	57.02	-222.6	20.72	-201.9
MH079	2352.00	31.40	-215.0	11.40	-203.6
MH010	1764.43	-31.11	-216.0	7.98	-208.0
RH020	1748.33	-32.70	-215.9	8.14	-207.8
RH030	1745.50	-32.85	-215.7	7.22	-208.5
RH040	1719.51	-36.33	-216.5	6.99	-209.5
RH050	1710.73	-37.89	-217.1	6.88	-210.2
RH060	1703.72	-39.58	-218.1	6.50	-211.6
RH070	1691.28	-41.59	-218.8	6.63	-212.2
RH080	1683.94	-42.85	-219.3	6.19	-213.0
RH090	1675.34	-44.29	-219.8	5.98	-214.4
RH110	1663.30	-46.58	-220.8	5.90	-214.9
RH120	1657.24	-47.71	-221.3	5.47	-215.8
RH130	1652.58	-48.74	-221.9	5.33	-216.6
RH140	1646.81	-49.91	-222.5	5.25	-217.3
RH150	1643.10	-50.95	-223.1	5.20	-217.9
RH160	1638.59	-52.68	-224.4	5.07	-219.3
RH170	1634.41	-53.23	-224.5	4.99	-219.5
RH180	1630.60	-54.35	-225.2	4.93	-220.2
MH009	1621.00	-59.21	-229.0	3.77	-225.2
MH154	1623.00	-61.24	-231.2	3.44	-227.8
MH151	1624.00	-62.47	-232.6	3.06	-229.5
MH148	1638.00	-62.78	-234.4	2.76	-231.6
MH170	1630.00	-62.23	-233.0	2.69	-230.3
MH171	1631.00	-62.05	-232.9	2.71	-230.2

APPENDIX III

Geothermal Gradient - Heat Flow Data

Temperature measurements, particularly in a geothermal environment, can be sensitive to the completion details of the observation borehole. Our measurements were made in shallow boreholes of 40 to 90 m depths drilled with hydraulic rotary equipment and consisted of two primary types: (1) coreholes and (2) rotary tricone holes. Coreholes were drilled into the volcanics occupying the east side of the Sevier fault with core being taken the entire length where recoverable. The rotary holes were drilled into the Quaternary alluvium on the west side of the fault with chip samples being taken from the mud flow line. Both hole types were drilled to a 12.0 cm diameter and completed with 2.54 cm black iron pipe that was sealed at the bottom. The annulus outside the black iron pipe was then grouted with cement to prevent vertical water circulation. After completion of the holes the black iron pipe was then filled with water and allowed to equilibrate to facilitate temperature measurements (better heat transfer between the measuring probe and surrounding rock).

Temperatures were measured repeatedly to 10 millidegrees at two meter inervals until all transient disturbances from drilling had vanished. A final equilibrium reading was then taken of the hole. Measurements were made on a four wire thermistor probe on loan from the USGS, with resistance across the thermistor measured to a precision of 1 with a portable digital multi meter. Resistances were then converted to temperatures in the field via tables based on a

calibration curve of the following form;

$$\log R = C + \frac{B}{T} + \frac{A}{T^2}$$

where R is resistance, T is temperature and A, B and C are calibration constants. Uncertainties in temperature measurements due to thermistor drift and calibration errors were determined to be negligible. Reproducibility of temperature measurements in the field were typically within .03°C.

Two different methods were used to measure the thermal conductivity of the drill samples. Conductivity measurements for the core were determined with a variant of the divided bar method (Birch, 1950) and found to have a precision of 4%. Thermal conductivities of drill cuttings were determined using the method described by Sass et al. (1971a, 1971b). This procedure involves packing crushed chips into a cell, water saturating them, measuring the aggregate conductivity on divided bar equipment and finally calculating the conductivity of the solid component from a geometric mean model.

The measured solid conductivity (K_s) from the chip method must be combined with estimates of the formation porosity (ϕ) to arrive at a conductivity of the formation (K_f). To calculate the conductivity of the alluvium an estimation of their porosity was made utilizing the resistivity data and Archie's law. This yielded a porosity of 32% which is in good agreement with estimated porosity listed for alluvial

gravels by Davis and DeWiest (1966) and Manger (1963). Formation conductivity was then calculated using a dispersive or Maxwell model

$$K_r = K_s \frac{(2r+1) - 2\phi(r-1)}{(2r+1) - \phi(r-1)}$$

where

$$r = \frac{K_s}{K_r}$$

The precision of this type of measurement was found to be 7%. The largest degree of error resides in the estimation of the porosity for the gravels. Errors of 10% in estimation of formation porosity will introduce an error of 11% in the formation conductivity.

The vertical component of heat flow, q, is computed as the product of the measured thermal conductivity and the vertical temperature gradient. Heat flow values were calculated directly from the product of the least-squares thermal gradient and mean conductivity for each of the bore holes. An estimate of the standard error residing in the heat flow value was made utilizing propagation of errors and the standard errors computed for the gradient and mean conductivity.

The topographic correction for heat flow was computed because of the rugged topography in the region; the plateau highlands obtain a relief of 2 km over the Sevier River valley within a horizontal distance of several kilometers. The topographic correction (Birch,

1950) to the temperature gradient for M6, the site that has the greatest topographic relief, amounts to 21% of the observed value. The above calculation is dependent on the regional geothermal gradient, and consequently on the regional heat flow for a given area. Since geothermal systems have large and locally variable heat flow, it is difficult to decide what value of average gradient is appropriate to use in the correction. The above calculation was made using the thermal gradient value at M6 (240 K km^{-1}) and is almost certainly too large. If a normal Basin and Range heat flow value of 80 mW m^{-2} is taken, this results in a gradient of 35 K km^{-1} and a topographic correction of only 3% to the gradient at M6. Topographic correction probably lies nearer the 3% value. M6 has by far the greatest relief around a site, so we may expect the error in the heat flow values due to the correction to be not more than 10% at the other sites.

Tabulations of the data for each hole is given in Tables 5 through 14. This data includes site location, elevation, temperature and conductivity measurements, summary geologic log and conductive heat flow. Each hole is accompanied with a figure (figures 16 through 25) graphically displaying this information.

Table 5

Location: Monroe
Borehole: M2

Conductivity: 231 $\pm$ .13
Gradient: 336 $\pm$ 4
Heat Flow: 775 $\pm$ 7

depth (m)	T (°C)	depth (m)	K (W m^{-1} °K^{-1})	to depth (m)	Geology
10	19.35	10	2.23	6	alluvium
12	20.25	15	2.24	61.8	Bullion Canyon
14	21.01	20	2.14		volcanics
16	21.80	25	2.48		
18	22.63	30	2.16		
20	23.41	35	2.41		
22	24.14	40	2.33		
24	24.93	45	2.21		
26	25.52	50	2.57		
28	26.42	55	2.42		
30	27.08	60	2.29		
32	27.75				
34	28.33				
36	28.99				
38	29.59				
40	30.36				
42	31.03				
44	31.67				
46	32.26				
48	32.90				
50	33.48				
52	34.09				
54	34.67				
56	35.25				
58	35.80				
60	36.29				
61.8	36.78				

Figure 16: Lithology, thermal conductivity and temperature profile for hole M2.

Table 6

Location: Monroe
Borehole: M3

Conductivity: $2.33 \pm .21$
Gradient: 725 ± 16
Heat Flow: 1689 ± 25

depth (m)	T (^{o}c)	depth (m)	K (W m^{-1} ^{o}K^{-1})	to depth (m)	geology
10	28.92	10	2.20	4	alluvium
12	30.73	15	2.29	72.5	Bullion Canyon
14	32.42	20	2.15		volcanics
16	34.21	25	2.22		
18	35.88	30	2.57		
20	37.52	35	2.81		
22	39.22	40	2.31		
24	40.62	45	2.25		
26	42.22	50	2.39		
28	43.56	55	2.31		
30	44.88	60	2.35		
32	46.15	65	2.56		
34	47.30	70	2.34		
36	48.55	75	2.29		
38	49.54				
40	50.54				
42	51.55				
44	52.60				
46	53.52				
48	54.51				
50	55.39				
52	56.20				
54	56.92				
56	57.58				
58	58.20				
60	58.70				
62	59.15				
64	59.56				
66	59.99				
68	60.47				
70	60.94				
72	61.47				
72.5	61.63				

Figure 17. Lithology, thermal conductivity and temperature profile for hole M3.

Table 7

Location: Monroe
Borehole: M4

Conductivity: $1.76 \pm .23$
Gradient: 615 ± 17 (10-40m)
Heat Flow: 1082 ± 23

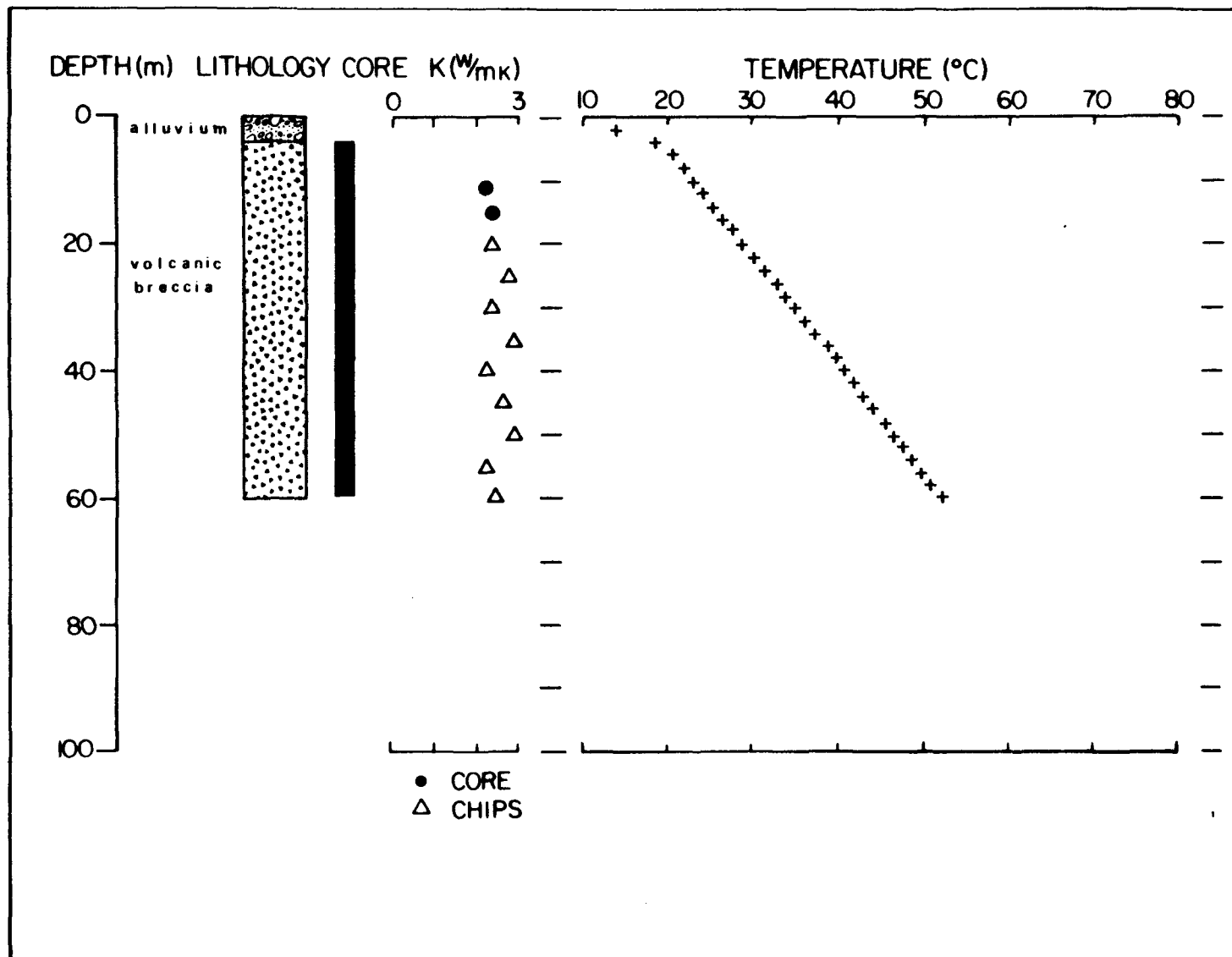| depth (m)	T (^{o}c)	depth (m)	K (W m^{-1} ^{o}K^{-1})	to depth (m)	geology
10	21.71	12.2	2.22	76.9	alluvium
12	23.20	18.3	1.61		
14	24.73	24.4	1.95		
16	26.09	30.5	1.61		
18	27.43	36.6	1.42		
20	28.64	42.7	1.70		
22	30.03	48.8	1.63		
24	31.35	54.9	1.95		
26	32.52	61.0	1.68		
28	33.65	67.1	1.82		
30	34.84	73.2	1.87		
32	35.84				
34	36.93				
36	37.89				
38	38.84				
40	39.76				
42	40.66				
44	41.54				
46	42.40				
48	43.26				
50	44.21				
52	44.94				
54	45.75				
56	46.50				
58	47.25				
60	47.86				
62	48.47				
64	49.08				
66	49.58				
68	50.08				
70	50.60				
72	51.06				
74	51.51				
76	51.91				
76.9	52.13				

Figure 18: Lithology, thermal conductivity and temperature profile for hole M4.

Table 8

Location: Monroe
Borehole: M5

Conductivity: $2.52 \pm .37$
Gradient: 739 ± 31
Heat Flow: 1836 ± 50

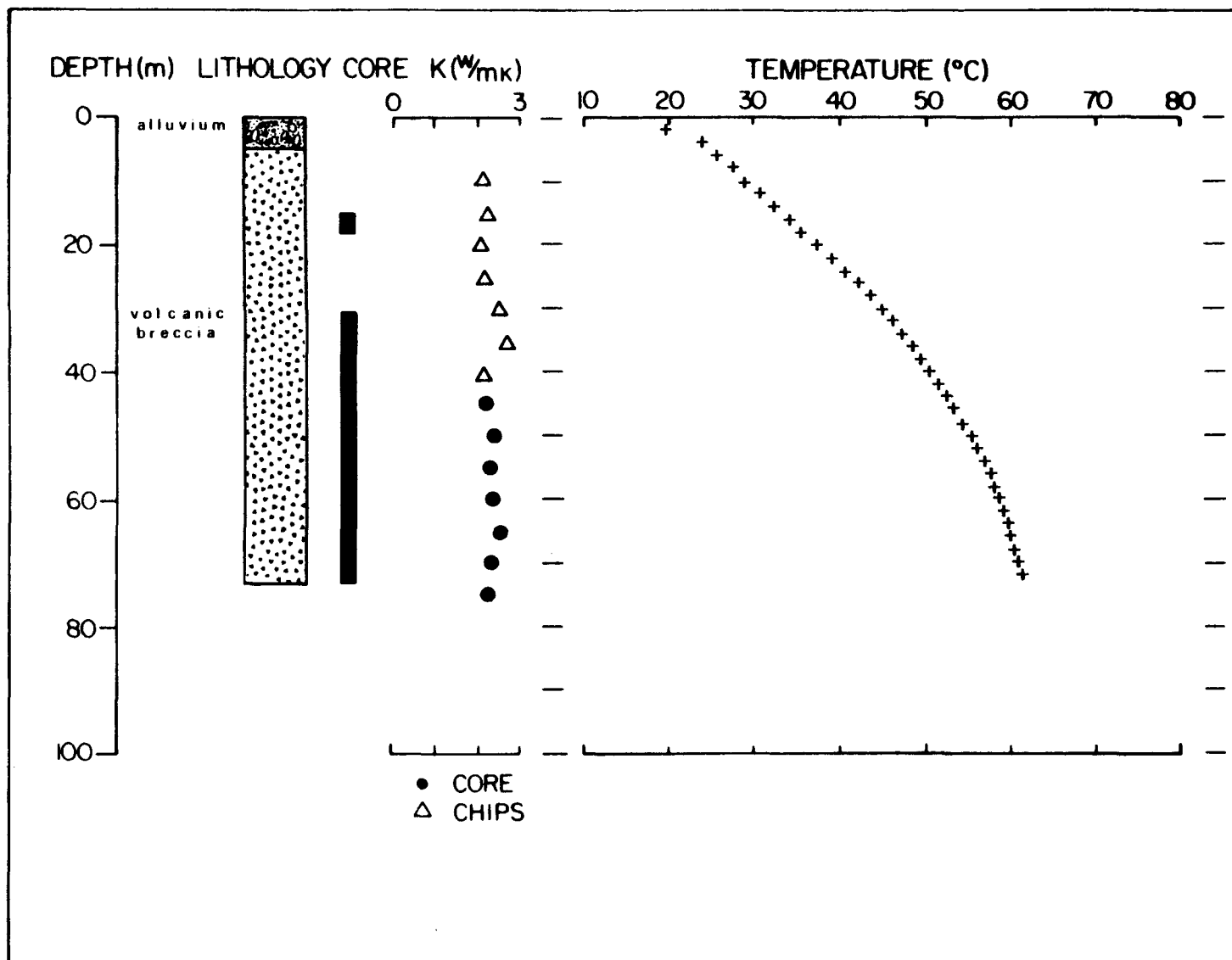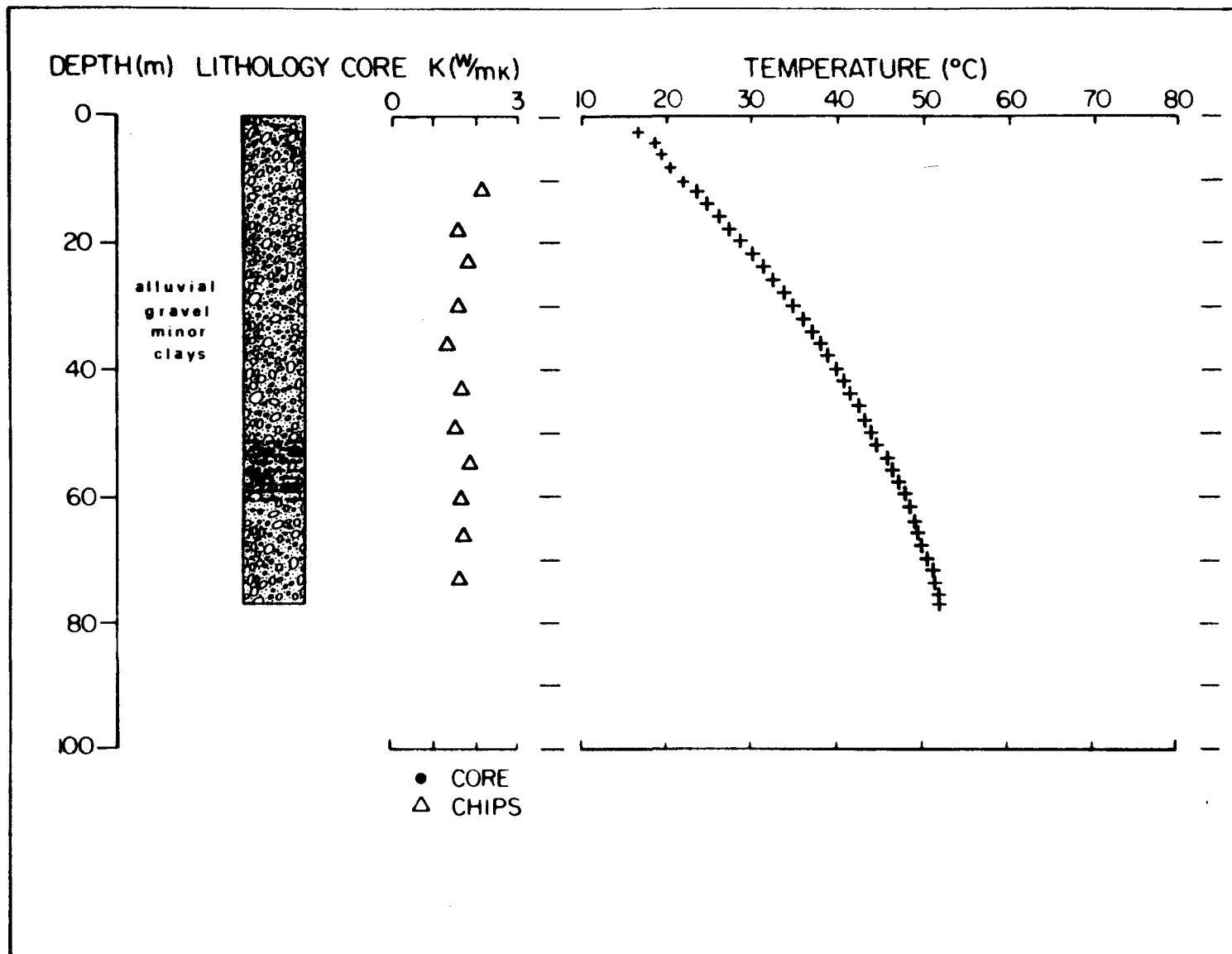| depth (m)	T (^{o}c)	depth (m)	K (W m^{-1} ^{o}K^{-1})	to depth (m)	geology
10	36.33	ND	2.98	38	Bullion Canyon
12	38.45	ND	2.04		volcanics
14	40.08	ND	2.70		
16	42.21	ND	2.60		
18	44.45	ND	2.26		
20	46.51				
22	48.03				
24	49.58				
26	50.97				
28	52.13				
30	53.22				
32	54.21				
34	55.19				
36	56.13				
38	56.87				

Figure 19: Lithology, thermal conductivity and temperature profile for hole M5.

Table 9

Location: Monroe
Borehole: M6

Conductivity: $2.30 \pm .24$
Gradient: 238 ∓ 2
Heat Flow: $548 - 5$

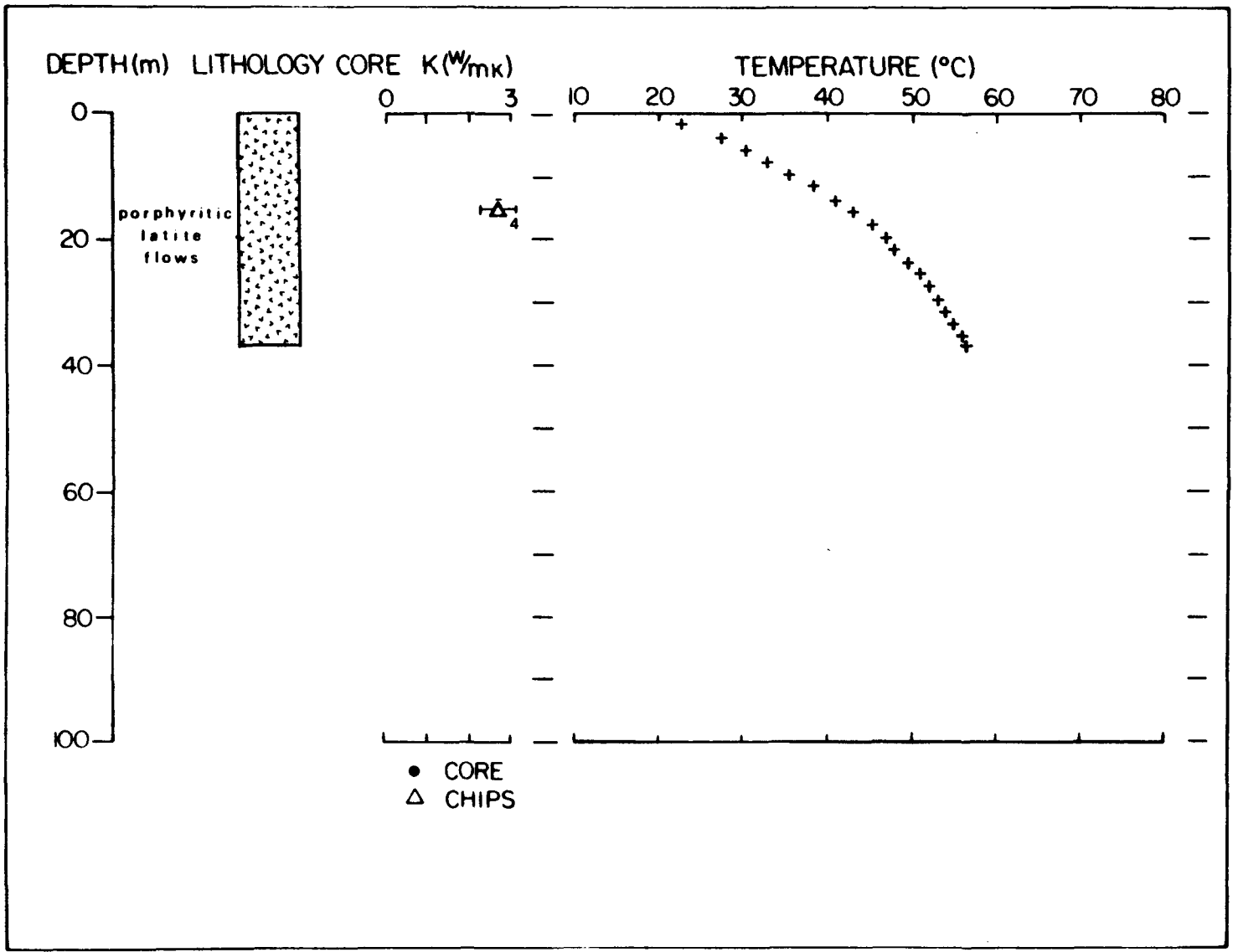| depth (m)	T (°c)	depth (m)	K (W m^{-1} °K^{-1})	to depth (m)	geology
10	16.62				
12	17.06	10	2.11	5	alluvium
14	17.55	15	2.49	75.8	Bullion canyon
16	18.09	20	1.78		volcanics
18	18.65	25	2.61		
20	19.18	30	2.27		
22	19.65	35	2.38		
24	20.15	40	2.23		
26	20.66	45	2.17		
28	21.16	50	2.75		
30	21.64	55	2.17		
32	22.09	60	2.30		
34	22.63	65	2.41		
36	23.12	70	2.40		
38	23.62	75	2.14		
40	24.11				
42	24.62				
44	25.08				
46	25.56				
48	26.04				
50	26.51				
52	26.92				
54	27.39				
56	27.80				
58	28.32				
60	28.78				
62	29.19				
64	26.63				
66	30.12				
68	30.52				
70	30.98				
72	31.42				
74	31.86				
75.8	32.21				

Figure 20: Lithology, thermal conductivity and temperature profile for hole M6.

Table 10

Location: Red Hill
Borehole: RH1

Conductivity: $2.52 \pm .24$
Gradient: 591 ± 2
Heat Flow: 1488 ± 7

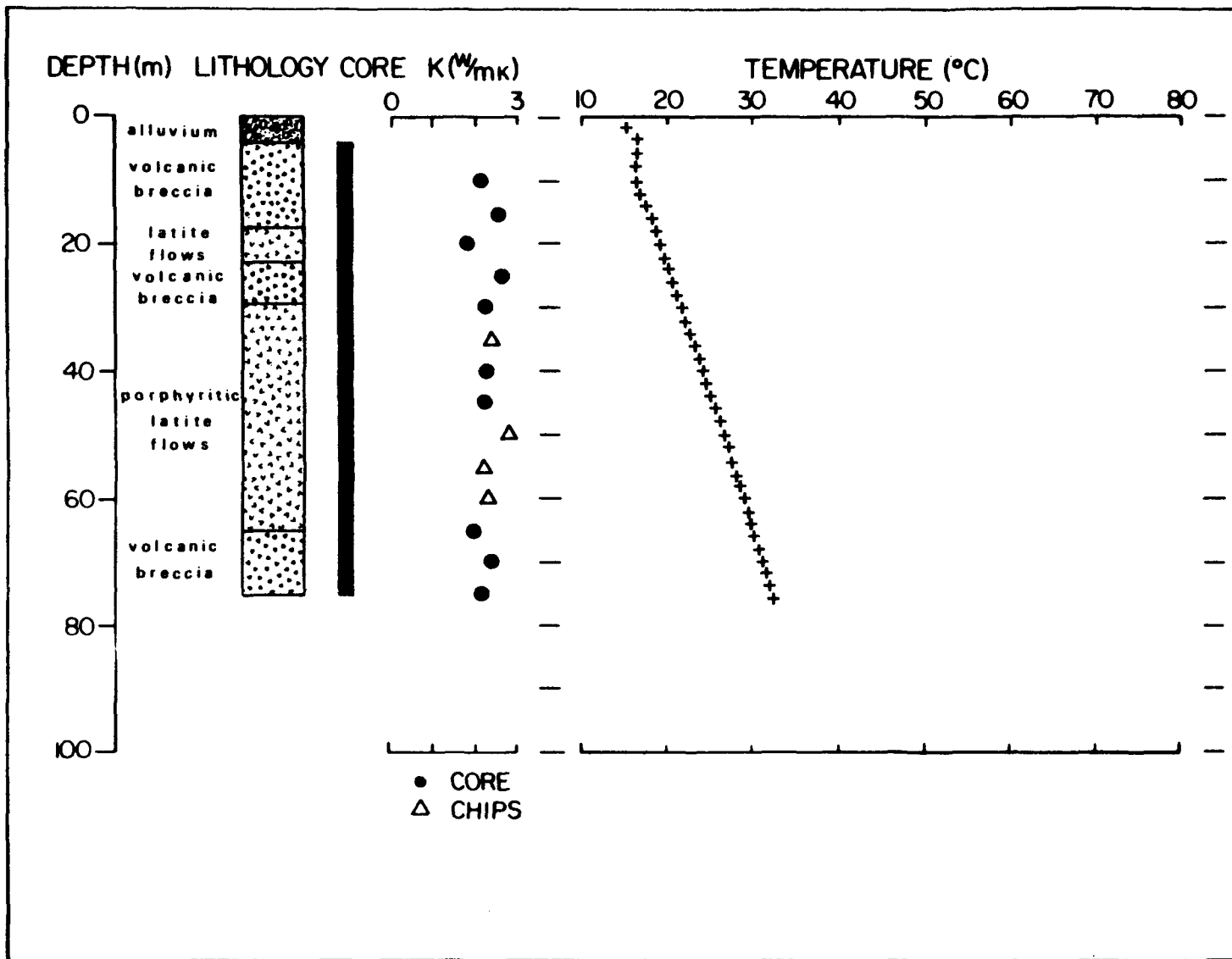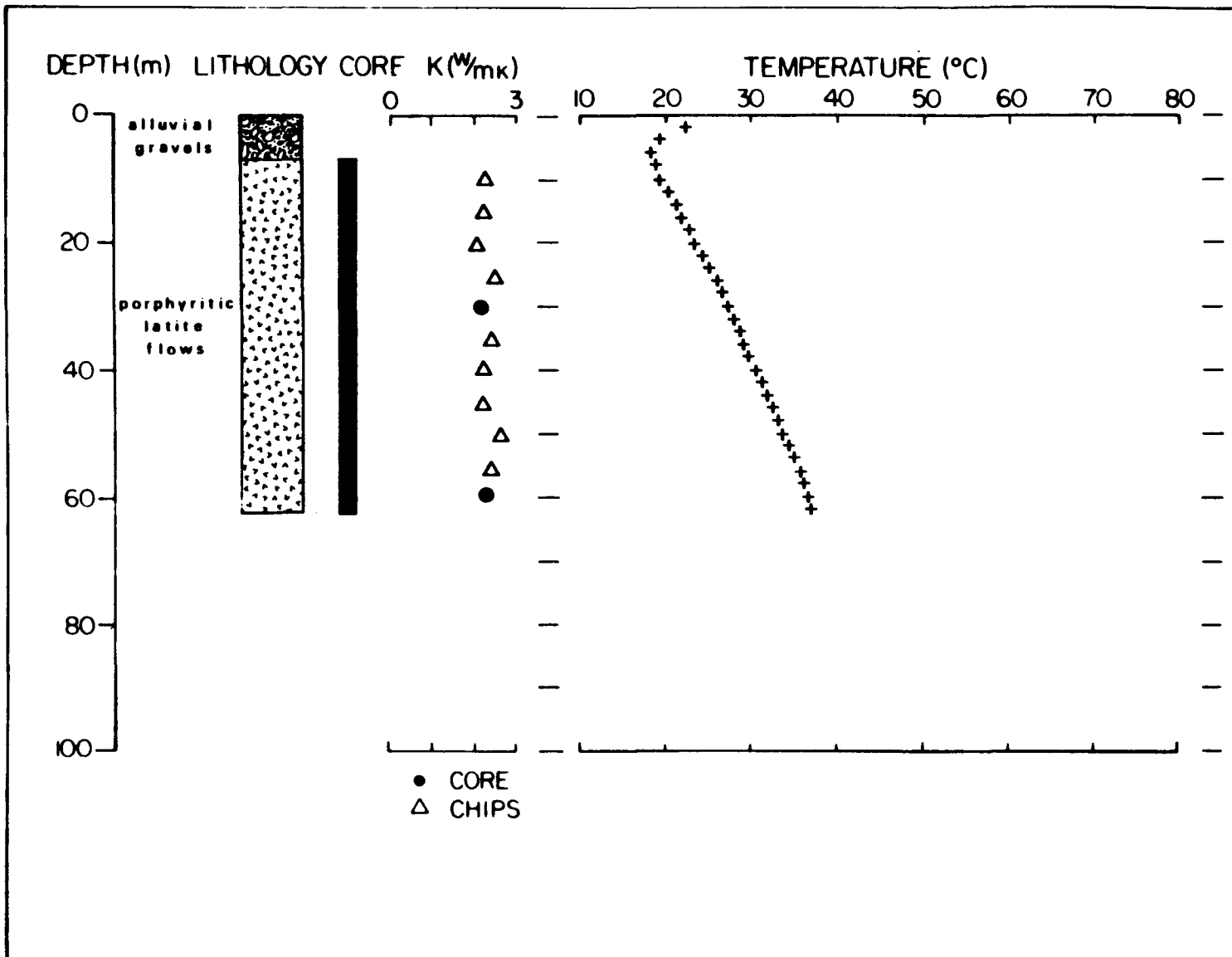| depth (m)	T (^{o}c)	depth (m)	K (W m^{-1} ^{o}K^{-1})	to depth (m)	geology
10	22.34	10	2.43	5	alluvium
12	23.95	15	2.38	60	Bullion Canyon
14	25.00	20	2.42		volcanics
16	26.32	25	2.79		
18	26.50	30	2.40		
20	28.79	35	2.91		
22	30.05	40	2.26		
24	31.06	45	2.65		
26	32.20	50	2.99		
28	33.43	55	2.24		
30	34.78	60	2.50		
32	35.97				
34	37.21				
36	38.49				
38	39.67				
40	40.63				
42	41.72				
44	42.87				
46	44.06				
48	45.27				
50	46.34				
52	47.59				
54	48.73				
56	49.80				
58	51.02				
60	52.12				

Figure 21: Lithology, thermal conductivity and temperature profile for hole RH1.

Table 11

Location: Red Hill
Borehole: RH2

Conductivity: 1.58 $\pm$ .35 water saturated .47 + .26 air saturated
Gradient: 7200 + 950 (0-10m)
Heat Flow: 3400 $\pm$ 650 air saturated

depth (m)	T (^{o}c)	depth (m)	K (W m^{-1} ^{o}K^{-1})	to depth (m)	geology
10	72.00	12.2	1.85	64	alluvium
12	72.20	18.3	1.85		
14	71.83	24.4	1.53		
16	71.04	30.5	1.62		
18	70.56	36.6	1.66		
20	70.20	42.7	1.50		
22	70.12	48.8	1.85		
24	70.46	54.9	1.78		
26	70.82	61.0	1.84		
28	71.24				
30	71.67				
32	72.00				
34	72.18				
36	72.36				
38	72.48				
40	72.56				
42	72.63				
44	72.60				
46	72.56				
48	72.51				
50	72.43				
52	72.34				
54	72.26				
56	72.18				
58	72.09				
60	72.08				
62	72.10				
64	72.14				

Figure 22: Lithology, thermal conductivity and temperature profile for hole RH2.

Table 12

Location: Red Hill
Borehole: RH 3

Conductivity: 1.49 $\pm$ .23
Gradient: 778 $\pm$ 10 (10-48m)
Heat Flow: 1160 $\pm$ 14

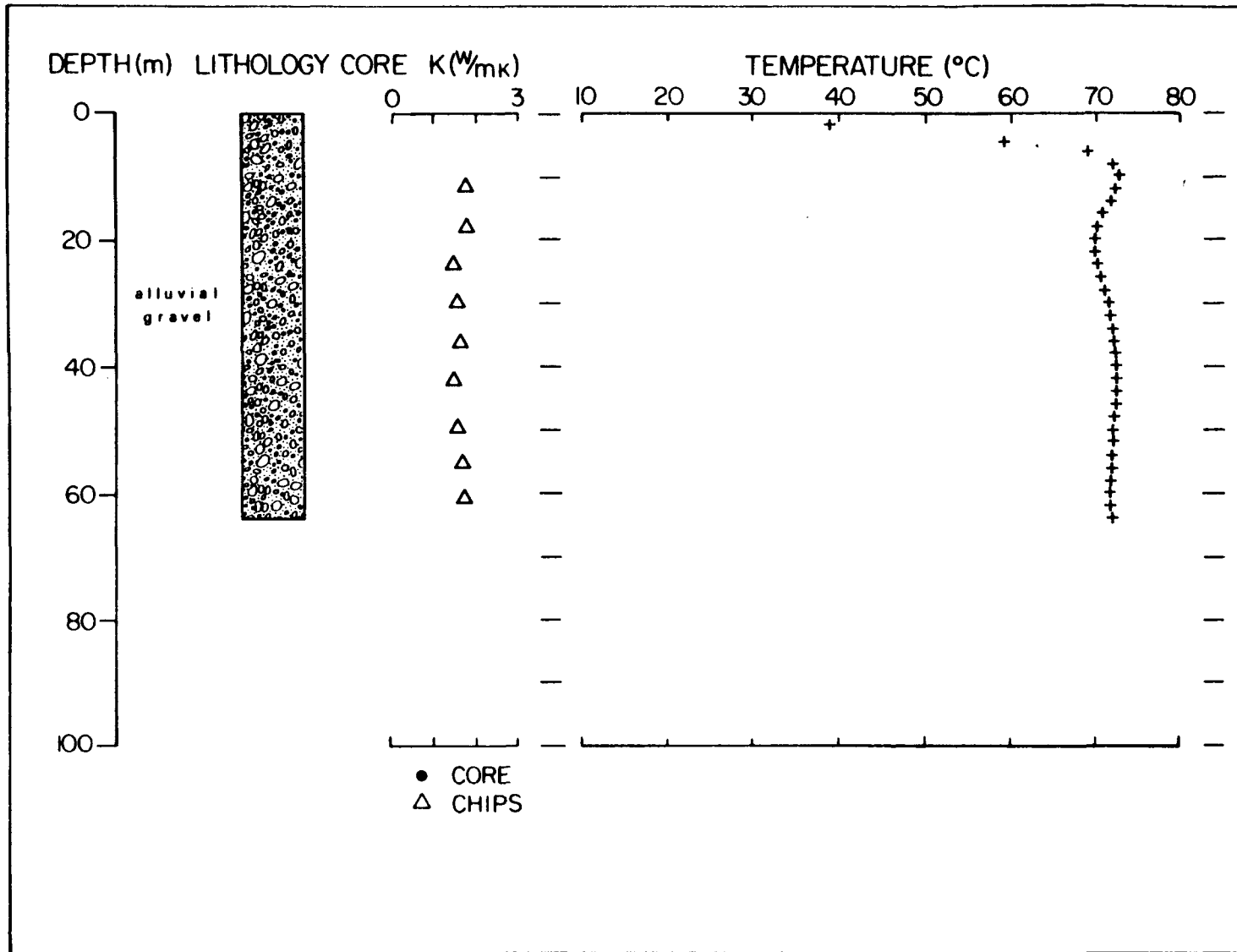| depth (m)	T (^{o}C)	depth (m)	K (W m^{-1} ^{o}K^{-1})	to depth (m)	geology
10	25.11	12.2	1.79	61.3	alluvium
12	27.16	18.3	1.65		
14	29.06	24.4	1.72		
16	30.86	30.5	2.09		
18	32.68	36.6	1.56		
20	34.48	42.7	1.60		
22	36.14	48.8	1.57		
24	37.95	54.9	1.60		
26	39.18	61.0	2.02		
28	40.94				
30	42.47				
32	43.92				
34	45.38				
36	46.93				
38	48.23				
40	49.62				
42	50.93				
44	52.34				
46	53.79				
48	55.08				
50	55.00				
52	55.23				
54	55.30				
56	55.80				
58	56.40				
60	56.73				
61.3	57.25				

Figure 23: Lithology, thermal conductivity and temperature profile for hole RH3.

Table 13

Location: Red Hill
Borehole: RH 4

Conductivity: 2.14 ± .19   .62 ± .34
Gradient: 5400 ± 710
Heat Flow: 3350 ± 560

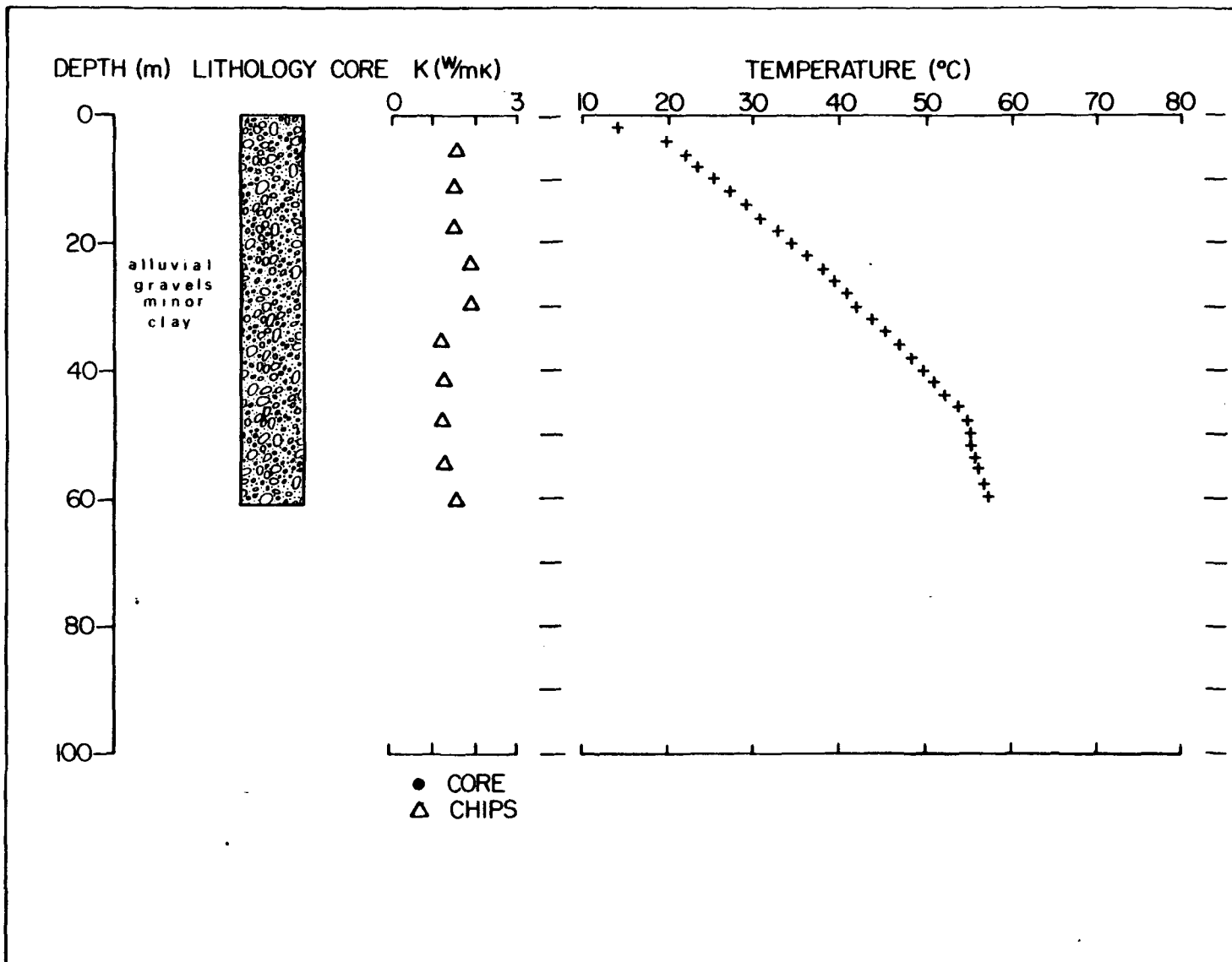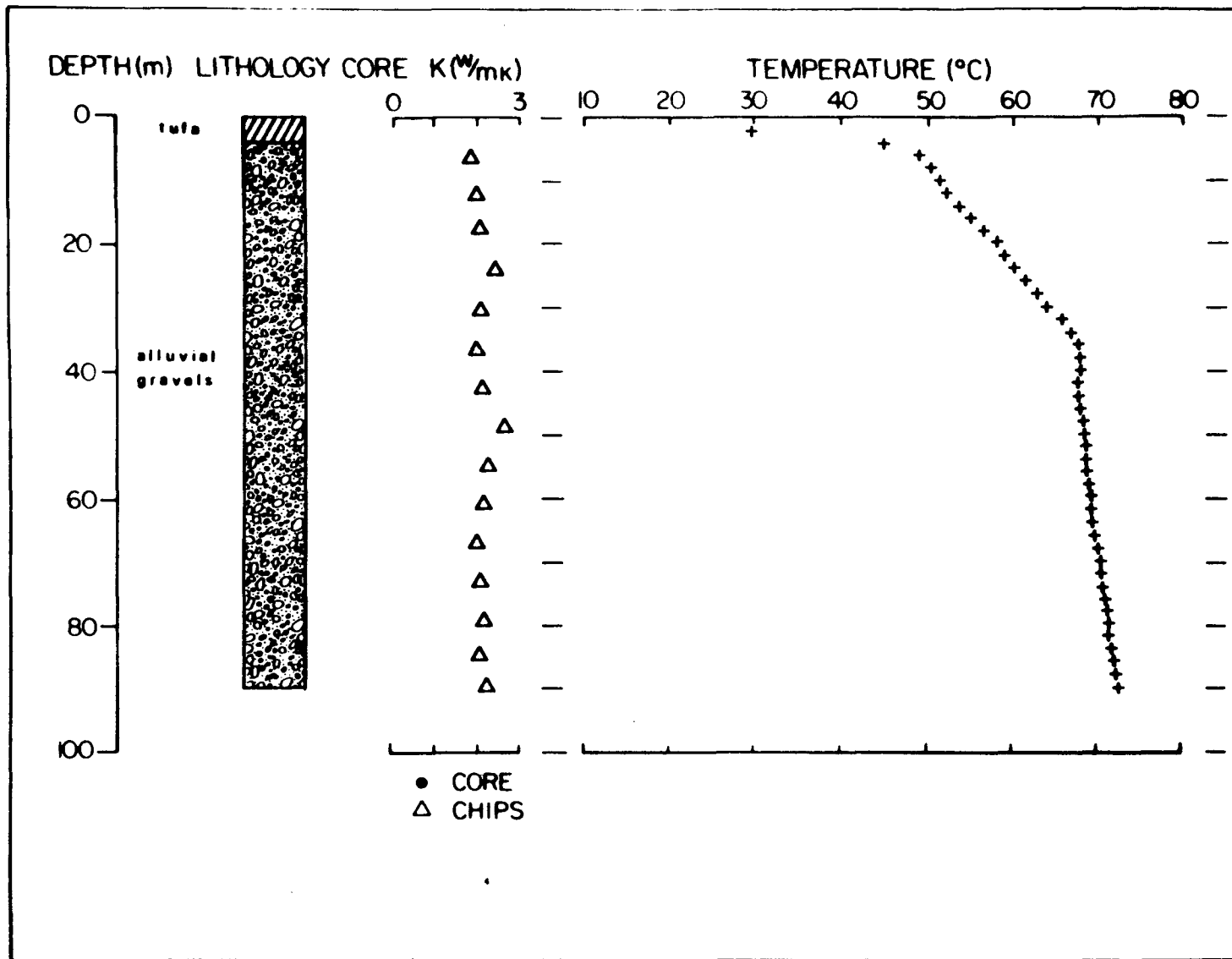| depth (m)	T (°c)	depth (m)	K (W m^{-1} °K^{-1})	to depth (m)	geology
10	50.71	6.1	2.00	14	alluvium with
12	52.10	12.2	2.76		travertine
14	53.50	18.3	2.87	90	alluvium
16	55.13	24.4	3.48		
18	56.56	30.5	2.91		
20	57.84	36.6	3.39		
22	59.08	42.7	2.97		
24	60.32	48.8	3.83		
26	61.62	54.9	3.18		
28	62.98	61.0	3.08		
30	64.07	67.1	2.79		
32	65.79	73.2	3.07		
34	67.44	79.3	3.10		
36	68.07	85.4	2.99		
38	67.98	91.5	3.11		
40	67.81				
42	67.71				
44	67.69				
46	67.76				
48	67.99	(temperatures			
50	68.27	continued)			
52	68.54	72	70.34		
54	68.63	74	70.43		
56	68.75	76	70.62		
58	68.93	78	71.07		
60	69.08	80	71.25		
62	69.31	82	71.53		
64	69.56	84	71.72		
66	69.77	86	71.96		
68	70.01	88	72.18		
70	70.24	90	72.31		

Figure 24: Lithology, thermal conductivity and temperature profile for hole RH4.

Table 14

Location: Red Hill
Borehole: RH 5

Conductivity: $1.38 \pm .10$ alluvium $2.12 \pm .06$ volcanics
Gradients: 628 ± 4 (10-46m)
Heat Flow: 866 ± 5

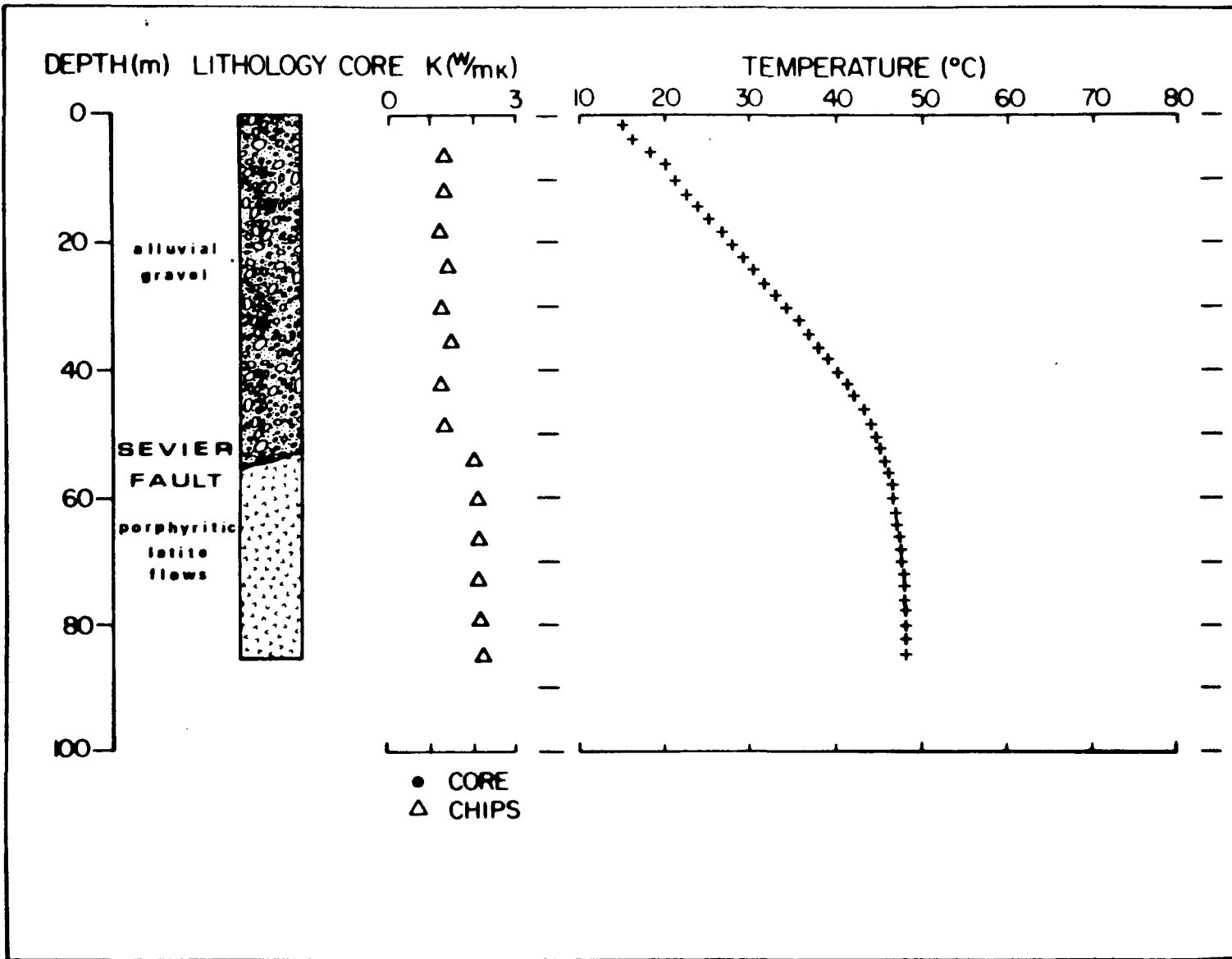| depth (m)	T (°C)	depth (m)	K (m⁻¹ °K⁻¹)	to depth (m)	geology
10	21.61	12.2	1.41	60	alluvium
12	22.87	18.3	1.30	84	Bullion Canyon
14	24.13	24.4	1.47		volcanics
16	25.26	30.5	1.32	60	Sevier fault
18	26.85	36.6	1.52		
20	28.21	42.7	1.38		
22	29.38	48.8	1.38		
24	30.58	54.9	2.14		
26	31.89	61.0	2.17		
28	32.20	67.1	2.18		
30	34.40	73.2	2.20		
32	35.68	79.3	2.30		
34	36.90				
36	38.10				
38	39.20				
40	40.40				
42	41.55				
44	42.45				
46	43.33				
48	44.13				
50	44.82				
52	45.44	(temperatures			
54	45.99	continued)			
56	46.46	72	48.05		
58	46.69	74	48.11		
60	46.90	76	48.17		
62	47.12	78	48.25		
64	47.42	80	48.35		
66	47.66	82	48.43		
68	47.82	84	48.57		
70	47.95				

Figure 25: Lithology, thermal conductivity and temperature profile for hole RH5.

APPENDIX IV

Dipole-Dipole Resistivity: Data Acquisition and Reduction

An in-line, 100m dipole-dipole electrode geometry was used.
Measurements were made at dipole separations of n=1,2,3,4. The
apparent resistivites have been plotted in pseudosections, figures 27
through 40, with each data point being plotted at the intersections of
two lines drawn at 45° from the centers of the transmitting and
receiving dipoles, figure 26.

The survey provides both resolution of vertical and horizontal
resistivity contrasts, since the field procedures generates both
vertical sounding and horizontal profiling measurements. Fourteen
traverse lines, totaling 20.6 km, were surveyed in a 40 km^2 region
along the Sevier fault. The lines comprise a dense network of
approximately .5 km spacing between lines in the Monroe-Red Hill area
to greater than 1 km spacings on the peripherals of the area.

Measurements were made in the frequency domain utilizing a
Geotronics model IP receiver and Geotronics model FT-20A transmitter.
A frequency of 1 Hz was used in order to minimize electromagnetic
coupling, while also minimizing observation time. Repeat measurements
were calculated on selected lines by interchanging the potential and
current dipoles to test the accuracy of the measurements. Average
percent differences were found to be approximately 11%, which is a
reasonable estimate of the error in the apparent resistivity value.

A three-wire power line extends north-south through the survey area. This structure acts as a grounded line source over a non-homogenous median, introducing 60 Hz noise and its harmonics. To minimize any spurious results resulting from redistribution of small amounts of current, dipole lines were run at right angles to the power line where topography permitted, and all measuring electrodes were kept out of close proximity with the poles. Changes in apparent resistivities that results from this type of structure have been estimated at under 10% (Nelson, 1977) for most surveys.
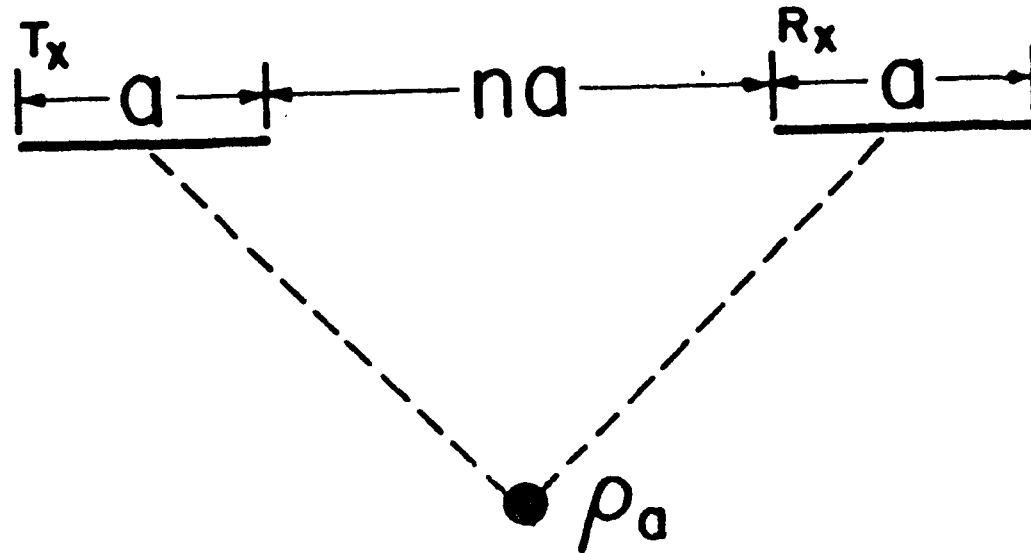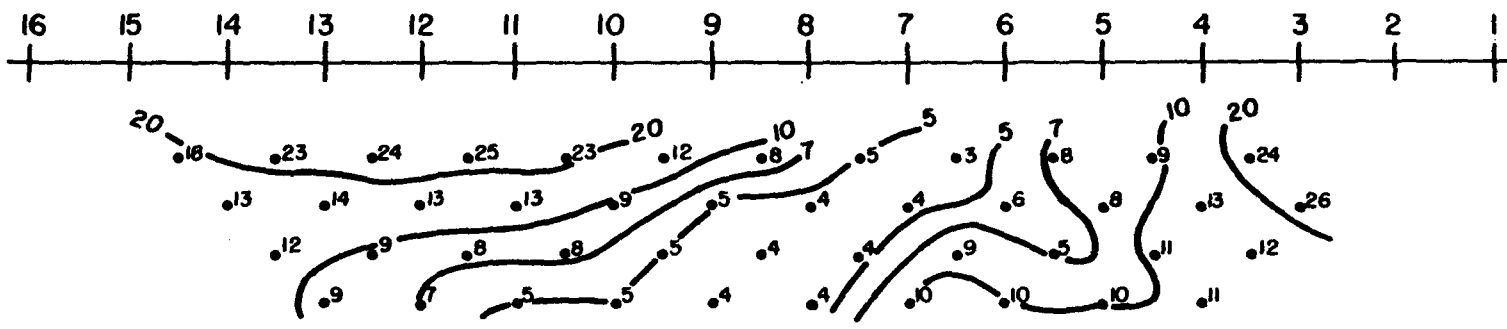
DATA PLOTTING SCHEME
DIPOLE-DIPOLE ARRAY

Figure 26

WEST   EAST

16   15   14   13   12   11   10   9   8   7   6   5   4   3   2   1

LINE M77-#1

PROJECT - MONROE
LOCATION - MONROE - RED HILL HOT SPRINGS
DIPOLE-DIPOLE RESISTIVITY - PSEUDOSECTION
a = 100m CONTOURS AT 1,2,3,5,10....

0   100   200   300   400   500
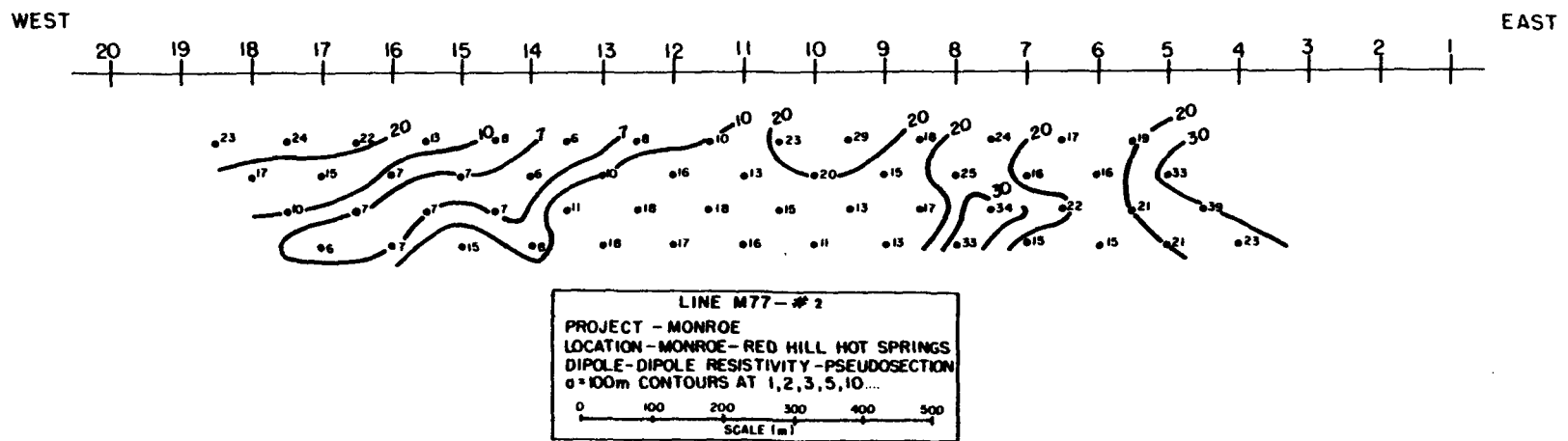SCALE (m)

Figure 27

WEST   EAST

LINE M77—# 2

PROJECT – MONROE
LOCATION – MONROE – RED HILL HOT SPRINGS
DIPOLE-DIPOLE RESISTIVITY – PSEUDOSECTION
a = 100m CONTOURS AT 1,2,3,5,10....

SCALE (m)

Figure 28

Figure 29

W 11 10 9 8 7 6 5 4 3 2 1 E

100 70 50   30   20

.153   .132   .156   115.   .41   .22   .23   .18

.128   .140   .96   .51   .38   21.   .15   .14

.122   118.   .76   .43   33.   .13   .18

112.   80.   .41   37   21.   .15

LINE M77 — # 4

PROJECT — MONROE
LOCATION — MONROE — RED HILL HOT SPRINGS
DIPOLE — DIPOLE RESISTIVITY — PSEUDOSECTION
a = 100m CONTOURS AT 1,2,3,5,10....

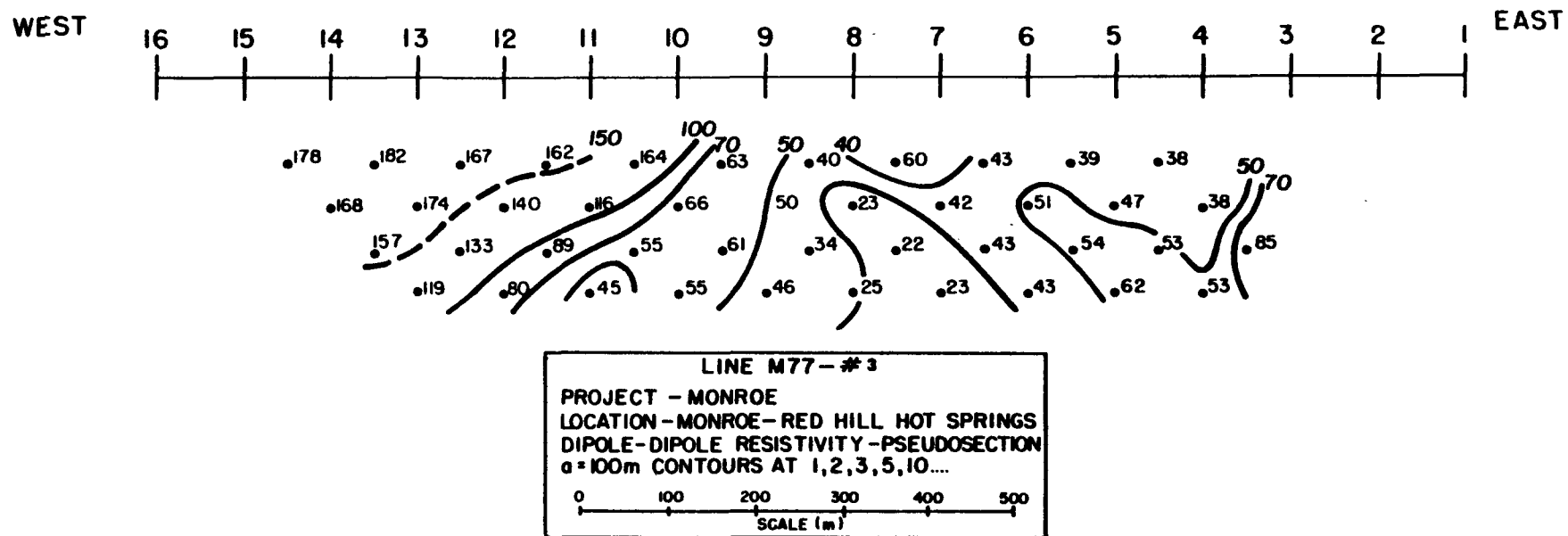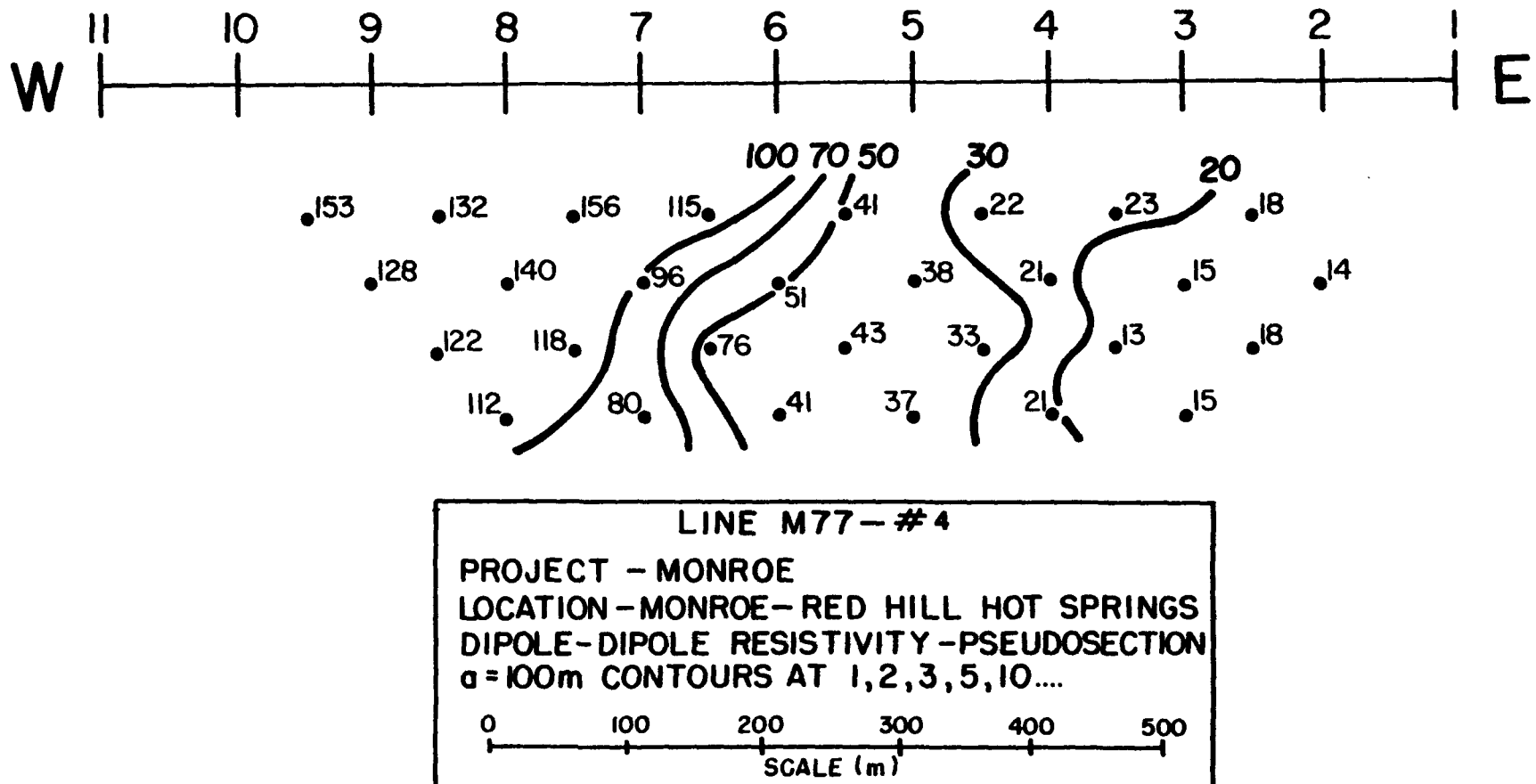0   100   200   300   400   500

SCALE (m)

Figure 30

W ‖ 11   10   9   8   7   6   5   4   3   2   1 ‖ E

30 50 70   100 70 50   30   20

20   •22   •28   •29   23•   •121   •92   •39   •22

10—•10   17•   •14   18••   •34   •19   •16   •14

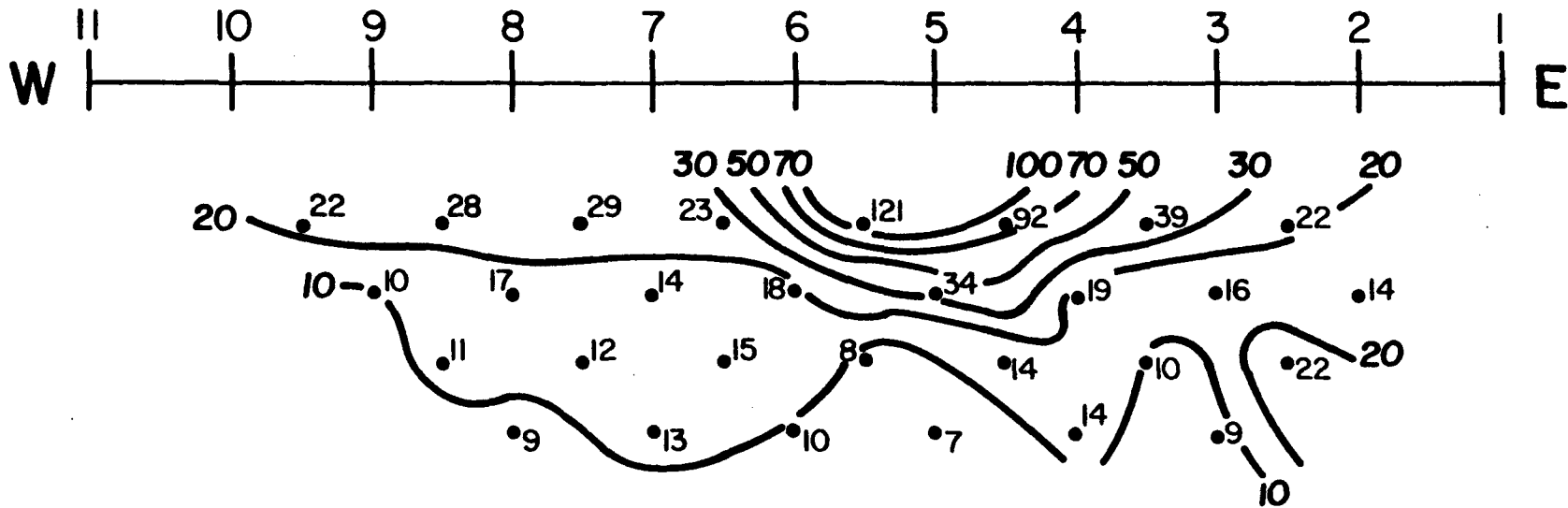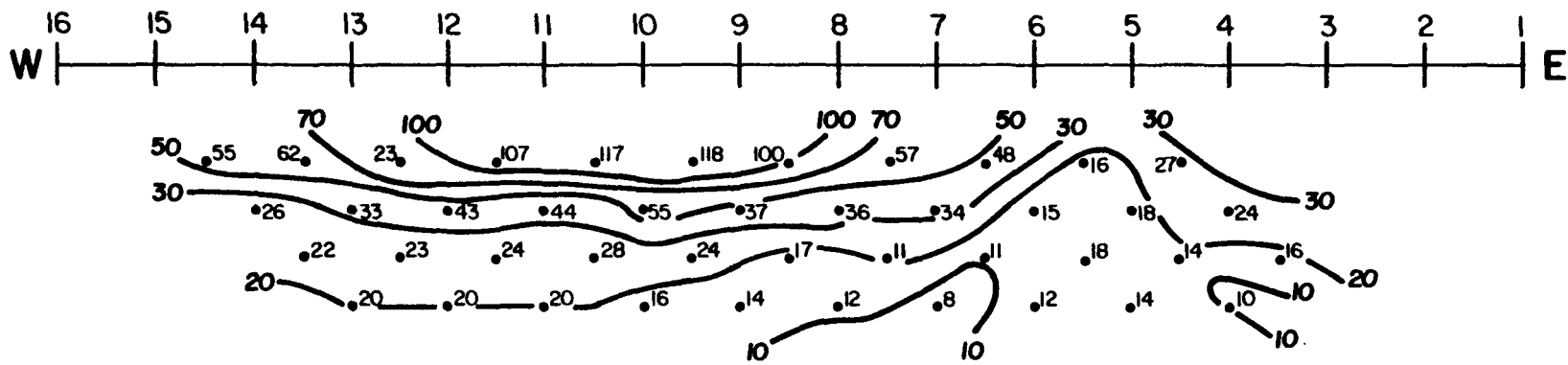•11   •12   •15   8••   •14   •10   •22   20

•9   •13   •10   •7   •14   •9
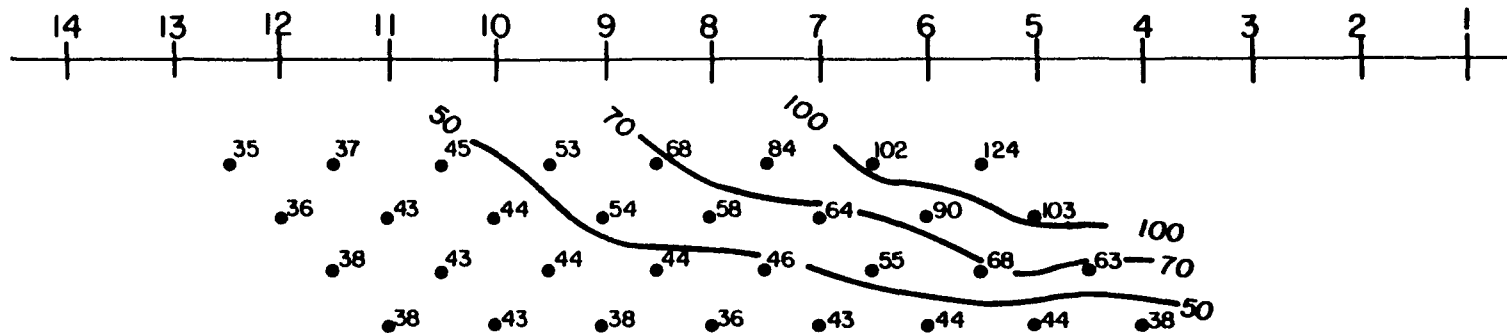
10

LINE M77—# 5

PROJECT — MONROE
LOCATION — MONROE — RED HILL HOT SPRINGS
DIPOLE-DIPOLE RESISTIVITY — PSEUDOSECTION
a = 100m CONTOURS AT 1, 2, 3, 5, 10....

0   100   200   300   400   500
SCALE (m)

Figure 31

Figure 32

Figure 33

Figure 34

W   18   17   16   15   14   13   12   11   10   9   8   7   6   5   4   3   2   1   E

70   70   100   100   70   70   70   50

67   85   82   85   89   56   108   78   65   62   63   85   56   41

50   50   51   52   57   52   64   61   48   46   50   60   52   47   36

46   41   45   41   42   42   42   54   40   44   36   42   43

40   41   38   38   32   33   32   33   34   27   32   40

30   30

LINE M77–#8

PROJECT – MONROE
LOCATION – MONROE – RED HILL HOT SPRINGS
DIPOLE-DIPOLE RESISTIVITY – PSEUDOSECTION
a = 100m CONTOURS AT 1,2,3,5,10....
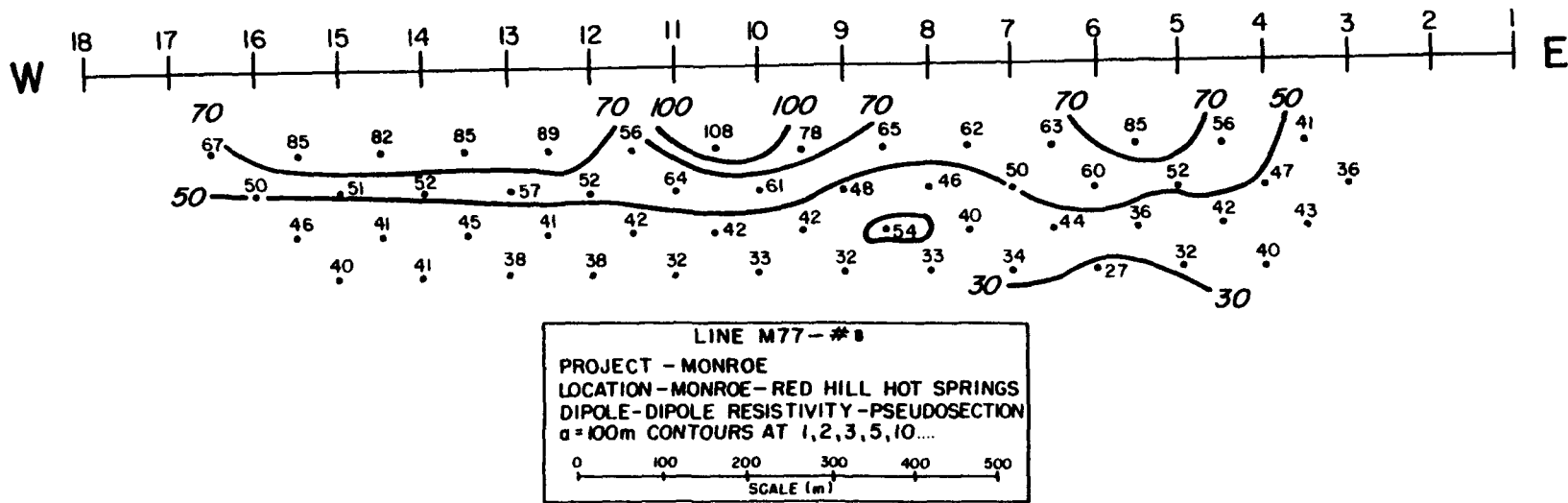
0   100   200   300   400   500
SCALE (m)

81

LINE M77-#10

PROJECT - MONROE
LOCATION - MONROE - RED HILL HOT SPRINGS
DIPOLE-DIPOLE RESISTIVITY - PSEUDOSECTION
a = 100m CONTOURS AT 1,2,3,5,10....

SCALE (m)

Figure 35

W   15   14   13   12   11   10   9   8   7   6   5   4   3   2   1   E

LINE M77 — # 14

PROJECT - MONROE
LOCATION - MONROE - RED HILL HOT SPRINGS
DIPOLE-DIPOLE RESISTIVITY - PSEUDOSECTION
a = 100m CONTOURS AT 1,2,3,5,10....
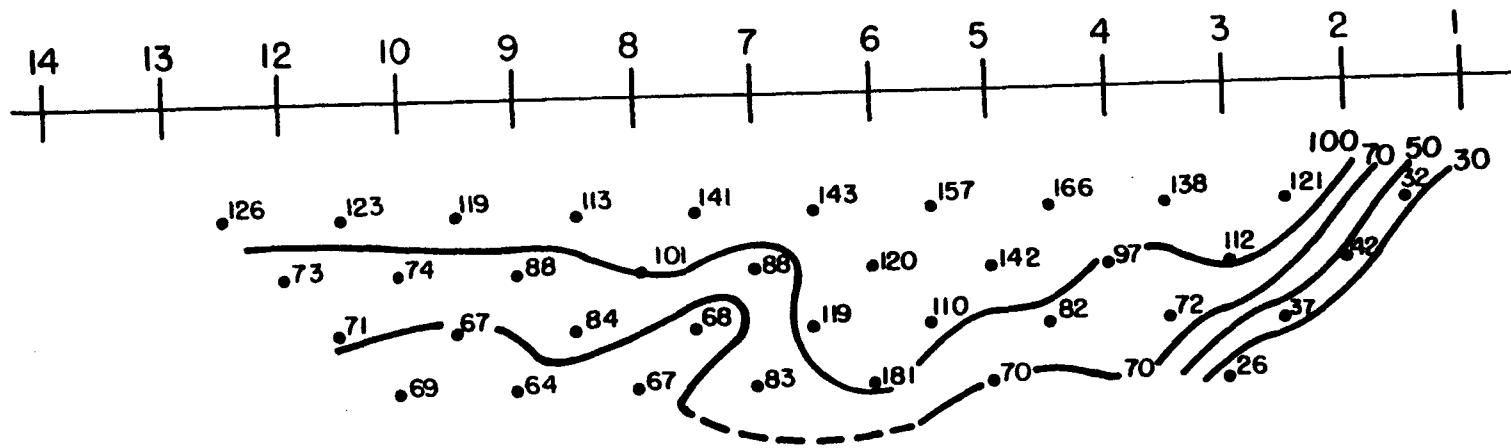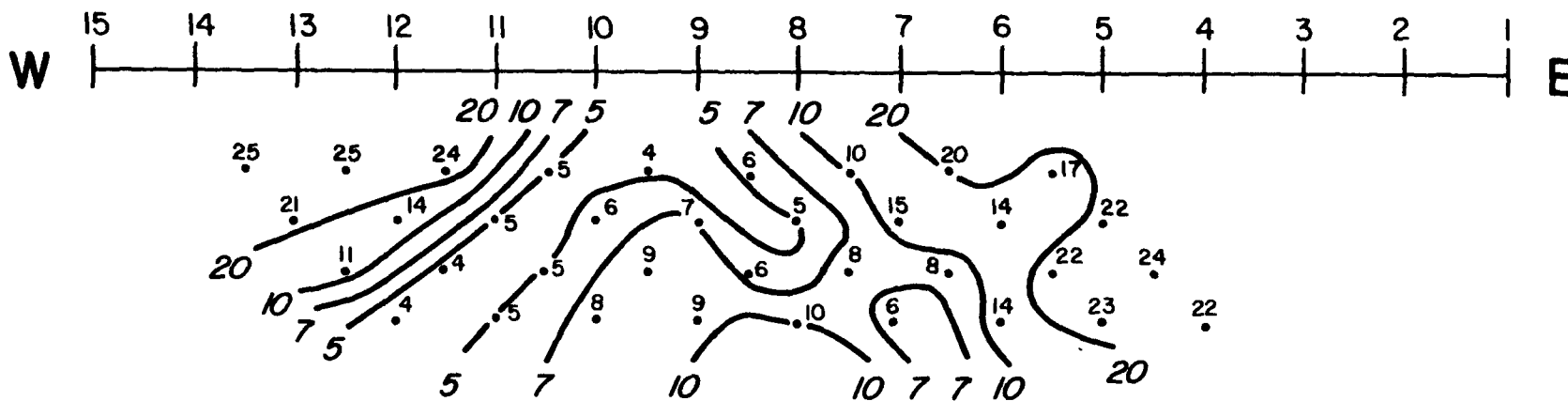
0   100   200   300   400   500
SCALE (m)

Figure 36

Figure 37

NW ⟼₁₇ ₁₆ ₁₅ ₁₄ ₁₃ ₁₂ ₁₁ ₁₀ 9 8 7 6 5 4 3 2 1⟼ SE

30   *20*   *20*

32   37   38   37   36   32   33   •27   21   12   15   23

30   19   18   •17   •17   •15   •15   •12   11   •9   11   11   17

20   12   11   12   10   •9   •8   •9   8   9   9   16   •14

•9   •9   8   7   •6   7   7   8   9   10   12   *20*

10   *7*   *7*   *10*

LINE M77—# 16

PROJECT — MONROE
LOCATION — MONROE — RED HILL HOT SPRINGS
DIPOLE-DIPOLE RESISTIVITY - PSEUDOSECTION
a=100m CONTOURS AT 1,2,3,5,10....
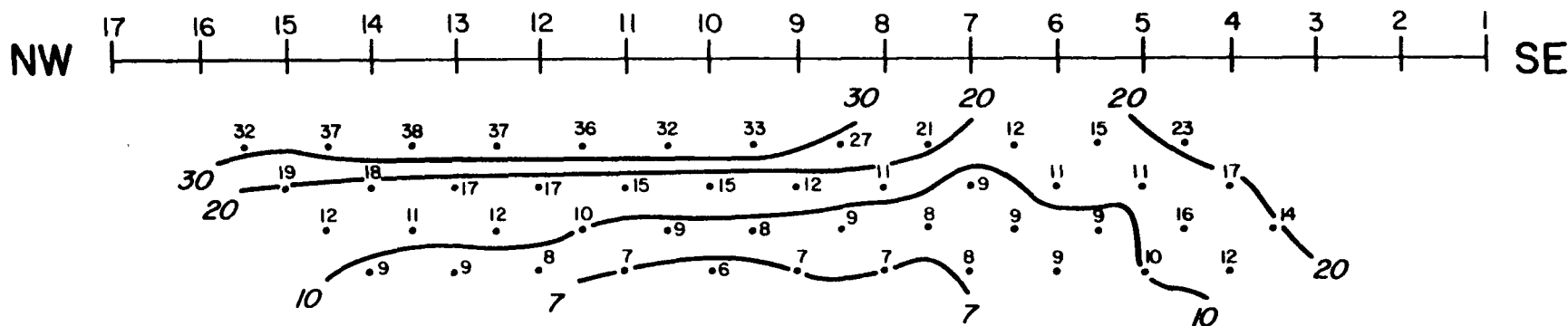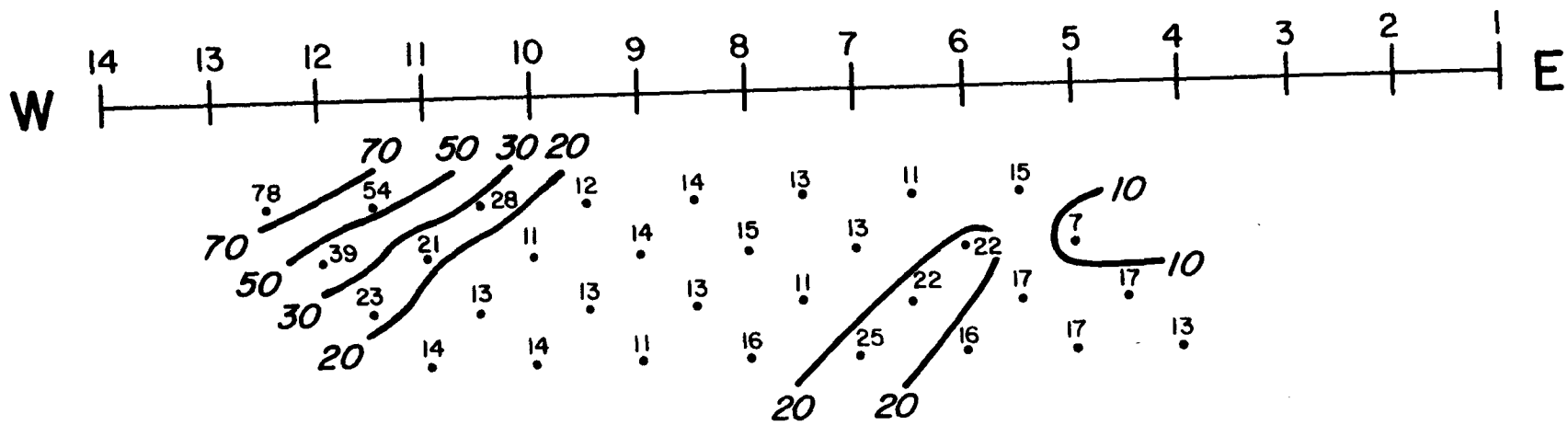
0   100   200   300   400   500
SCALE (m)

Figure 38

LINE M77—#17

PROJECT — MONROE
LOCATION — MONROE — RED HILL HOT SPRINGS
DIPOLE-DIPOLE RESISTIVITY-PSEUDOSECTION
a=100m CONTOURS AT 1,2,3,5,10....

SCALE (m)

Figure 39

WEST   EAST

15   14   13   12   11   10   9   8   7   6   5   4   3   2   1

LINE M77—#18

PROJECT – MONROE
LOCATION – MONROE – RED HILL HOT SPRINGS
DIPOLE-DIPOLE RESISTIVITY – PSEUDOSECTION
a = 100m CONTOURS AT 1,2,3,5,10....

0   100   200   300   400   500
SCALE (m)
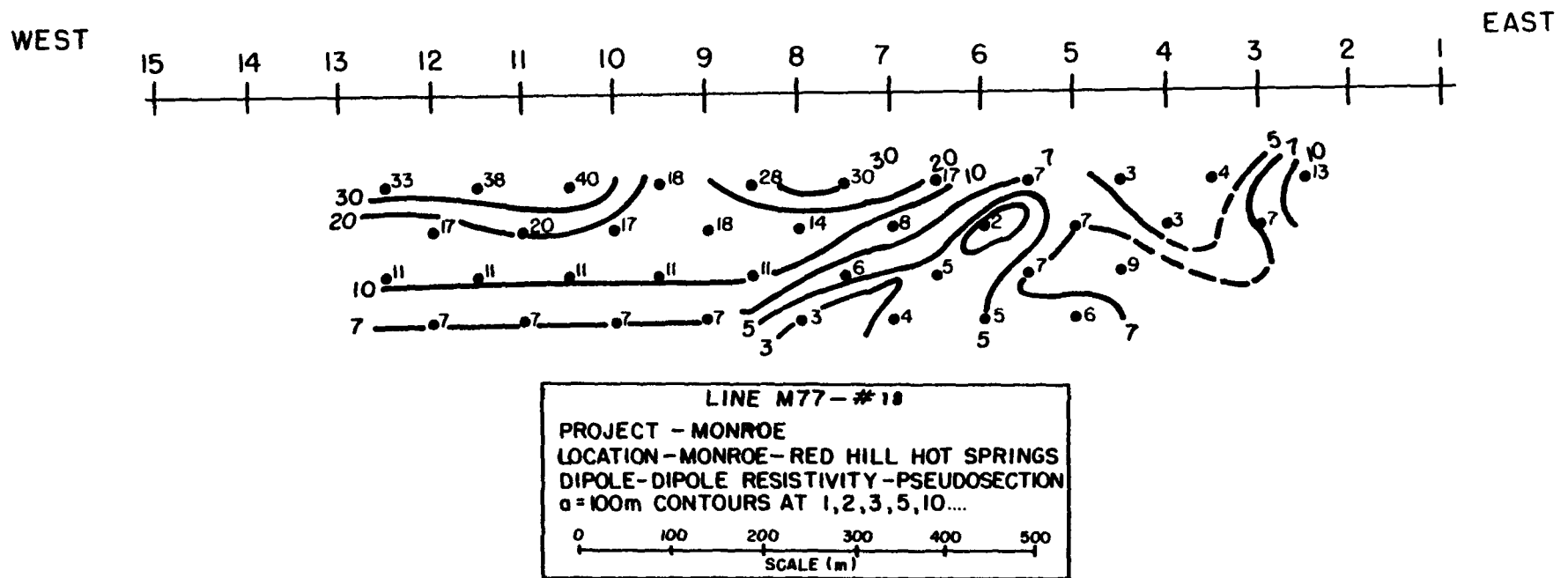
Figure 40

REFERENCES

Birch, F., 1950. Flow of heat in the Front Range, Colorado. Geol.
    Soc. Am. Bull., 61; p. 567-630.

Blackwell, D. D., Chapman, D. S., 1977. Interpretation of Geothermal
    Gradient and Heat Flow Data for Basin and Range Geothermal
    System. Geothermal Resources Council, TRANSACTIONS, 1; 19-20.

Brace, W. F., 1977. Permeability from resistivity and pore shape,
    Jour. Geophysical Research, 82, p. 3343-3349.

Callaghan, E. and Parker, R., 1961. Geologic map of the Monroe
    Quadrangle, Utah. U.S. Geol. Survey.

Davis, S. N. and DeWist, R. J., 1966. Hydrogeology. John Wiley and
    Sons, Inc., New York.

Hahl, D. C. and Mundroff, J. C., 1968. An appraisal of the quality of
    surface water in the Sevier Lake Basin, Utah, 1964. State of
    Utah Dept. of Natural Resources Tech. Publ. No. 19.

Halliday, M. E., 1978. Gravity and ground magnetic surveys in the
    Monroe and Joseph Known Geothermal Resource Areas and surrounding
    region, south-central Utah. Dept. of Geol. and Geophys. M.S.
    Thesis, University of Utah.

Hardy, C. T., 1952. Eastern Sevier Valley and Sanpete Counties, Utah.
    Utah Geological and Mineralogical Survey Bull., H3.

Keller, G. V. and Frischneckt, F. C., 1966. Electrical Methods in
    Geophysical Prospecting. Permagon Press. Oxford.

Kilty, K., Chapman, D. S., and Mase, C., 1978. Aspects of forced
    convective heat transfer in geothermal systems. Dept. of Energy,
    Division of Geothermal Energy, Contract No. EG-78-C-07-1701,
    University of Utah.

Lachenbruch, A. H., Sorey, M. L., Lewis, R. E., and Sass, J. H., 1976.
    The near-surface hydrothermal regime of Lony Valley caldera.
    Jour. Geophysical Research, 81; p. 763-768.

Manger, G. E., 1963. Porosity and bulk density of sedimentary rocks.
    U.S. Geol. Survey, Bull. 1144-E.

Miller, C. D., 1976. Aleration and geochemistry of the Monroe Known

Geothermal Resource Area. Dept of Geol. and Geophys., M.S. Thesis, University of Utah.

Nelson, P. H., 1977. IP effects from grounded structures. Geophysics, 42, No. 6, p. 1241-1253.

Parry, W. T., Benson, N. L., and Miller, C. D., 1976. Geochemistry and hydrothermal alteration at Selected Utah hot springs. National Science Foundation, Contract No. GI-43741, Vol. 3, University of Utah.

Sass, J. H., Lachenbruch, A. H., and Munroe, R. J., 1971(a). Thermal Conductivity of rocks from measurements on fragments and its application to heat flow determinations. Jour. of Geophysical Research, 76; p. 3391-3401.

Sass, J. H., Lachenbruch, A. H., Munroe, R. J., Greene, G. W., and Moses, T. H., Jr., 1971(b). Heat flow in the Western United States. Jour. Geophysical Research, 76, p. 6376-6413.

Stokes, W. L., and Hintze, L. F., 1963. Geologic Map of Utah, Southwest quarter.

Ward, S. H., and Sill, W. R., 1976. Dipole-dipole resistivity surveys, Roosevelt Hot Springs KGRA. National Science Foundation Contract No. GI-43741, Vol. 2, University of Utah.

Wilson, W. R., and Chapman, D. S., 1978. Personal Communication.

Young, R. A., and Carpenter, C. H., 1965. Groundwater conditions and storage in the central Sevier Valley, Utah. U.S. Geol. Survey Water Supply Paper 1787.